EXTENDING YIELD-STRESS FLUID PARADIGMS

BY

ARIF Z. NELSON

THESIS

Submitted in partial fulfillment of the requirements
for the degree of Master of Science in Mechanical Engineering
in the Graduate College of the
University of Illinois at Urbana-Champaign, 2015

Urbana, Illinois

Advisor:

Assistant Professor Randy H. Ewoldt

ABSTRACT

In this thesis, we present two new paradigms for yield-stress fluids; the first organizes the existing understanding of the various ways to achieve a yield-stress fluid into a useful methodology for the design of rheologically complex materials; the second is based on the discrepancy in the behavior in extension of model yield-stress fluids versus application-relevant materials. Through implementation of material design principles of selection and synthesis, yield-stress fluid microstructures are organized according to the two known mechanical interactions capable of producing them (jamming and attraction). This rheology-to-structure inverse problem reveals trade-offs in designing yield-stress fluids, demonstrating that multiple material classes can achieve a target yield stress, providing the opportunity for creative design to achieve both the yield stress and other secondary design criteria. A secondary design criteria that is investigated in depth here is extensibility. We introduce a method for characterizing the extensibility of yield-stress fluids, demonstrate the extent to which existing model materials differ from the high extensibility seen in real yield-stress fluids (commercial products, biomaterials), and introduce an attempt at creating a model material for highly-extensible yield-stress fluids.

ACKNOWLEDGEMENTS

I thank my family and friends for their love and support during my work. I also thank my advisor, Dr. Randy Ewoldt, for his indefatigable mentorship. Thanks goes to my former undergraduate assistants Jennifer Lin and Sean Hidaka for their experimental work. I especially thank Rebecca Corman and all of the rest of the Ewoldt Research Group, Ritu Raman, and Anna Oldani for their help and all of the fun along the way. Thank you to Rafael Bras, Eric Klingenberg, Leslie Morgret, Jingping Liu, and Wm. Wrigley Jr. Company for supporting the research presented in this thesis.

TABLE OF CONTENTS

CHAPTER 1: Introduction

The rheologically complex phenomenon of the yield-stress fluid, the transition from solid-like to liquid-like behavior upon a critical applied stress [1], is utilized throughout daily life and industry. The concept applies to products that many use every day such as peanut butter and toothpaste, but is also extremely important for a multitude of industrial applications such as the manufacturing of foodstuffs and 3D printing [2–4]. It is no surprise then that yield-stress fluids have been the subject of substantial rheological characterization and study [1,2,5,6].

This thesis, which focuses on yield-stress fluids, will apply design theories to rheologically complex materials in order to develop a methodology for the selection and creative synthesis of yield-stress fluids that is useful for design and is based on the comparison of secondary design objectives, organize a useful design database for material structures that can produce a yield stress, and show that this has the potential as a generic methodology for the material-level design of other rheological properties (Chapter 2). The secondary design objective of high-extensibility will then be considered, and a method for characterizing the extensibility of yield-stress fluids will be introduced. Using this method, the extent to which model materials differ from application-relevant materials in terms of extensibility will be demonstrated. These two complementary design and analysis/characterization methods (shown schematically in Figure 1.1) are used for the introduction of a simply formulated material that is both highly-extensible and has a yield-stress (Chapter 3).

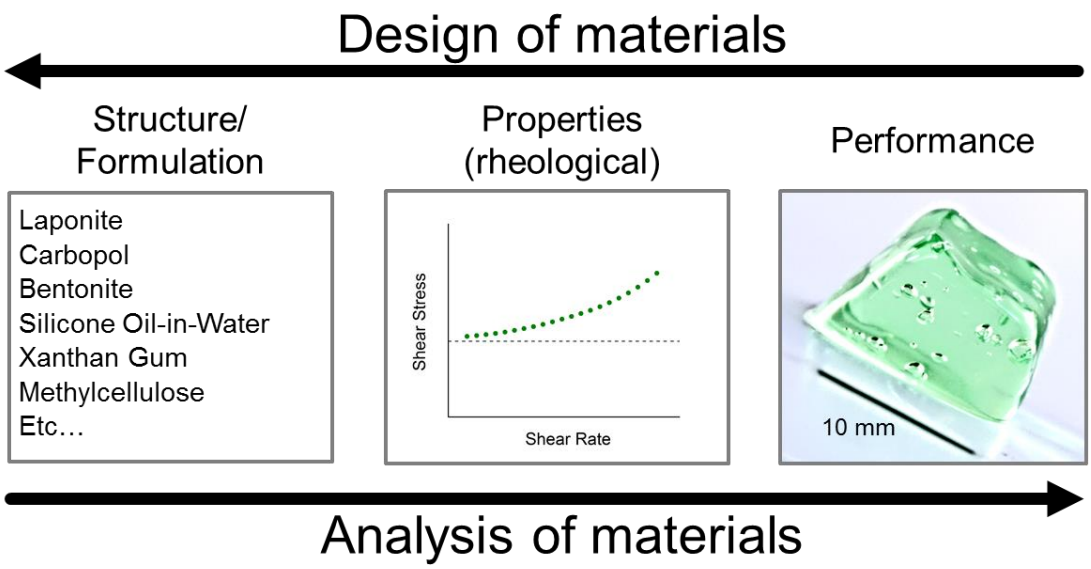

Figure 1.1. Design is the inverse of analysis (adapted from [7] and applied to rheological properties). Analysis starts with a specific material structure and connects it to properties and performance which is non-trivial for rheologically-complex materials. Design starts with a desired performance (e.g. shape-holding with a yield-stress fluid), and a decision is made on what material to best achieve it. Image from [8].

CHAPTER 2: Design of Yield-Stress Fluids

2.1 Introduction

Rheologically complex fluids have the potential to be utilized to a much greater degree in solving engineering design problems. These materials are ubiquitous in biological systems and the novel behavior could be used to meet numerous and diverse design objectives [8]. Without a doubt, currently the most utilized rheological phenomenon is the yield-stress fluid, the transition from solid-like to liquid-like behavior upon a critical applied stress. The importance of yield-stress fluids in daily life and industry cannot be understated as the concept applies to products as pedestrian as paint and toothpaste but also to applications as esoteric as crude oil gelation and rocket fuel [1,2]. In the development of a new processing technique for making tailorable ceramic beads, a yield stress was found to be a sufficient rheological property since it enabled shear-reversible plastic deformation [9]. In the food industry, the yield stress is of great importance for processing, manufacturing, and functional properties, as well as for correlation with sensory indices [3]. In 3D printing applications, the yield stress has been taken advantage of both for inks that will hold their extruded shape for cellular composites [4], and for a medium in which to print large complicated structures with microscopic precision [10]. For biomedical applications, an emerging paradigm of moldable hydrogels is based on the material being a yield-stress fluid capable of drug delivery [11]. For design of all these materials, the primary design objective is a material that has a yield stress since that is what enables the novel behavior. Therefore, before considering any constraining secondary objectives (e.g. biocompatibility), design of these materials should consider all the possible ways the yield stress might be achieved

since for this primary objective it is the functionality that matters not the chemistry that achieves it [12].

However, in the field of rheology, most efforts focus on the *analysis* of materials rather than facilitating more useful *design* practices and methodologies. By *analysis*, we mean that, starting with known ingredients or a known microstructure, a material is characterized and these properties are related to the macroscopic performance. To *design* a material is the inverse of this analysis process; starting with the desired macroscopic performance, decisions must be made on what properties might achieve that objective, and in turn what ingredients or microstructure might result in those properties. A schematic of the complementary analysis and design perspectives is shown in Figure 1.1. For rheological materials, the analysis/characterization of material properties can be especially arduous due to their function-valued nature. An example of the structure-to-rheology organization that results from the analysis approach is shown in Figure 2.1; a single material, an emulsion, has several complicated structural and observational dependencies.

As stated previously, there are few, if any, efforts to apply materials design theories to rheologically complex materials; our goals here are to (i) demonstrate the adaptation of generic theories of materials selection and synthesis to yield-stress fluids, (ii) organize a useful design database for material structures that can produce a yield stress i.e. organize known (design) strategies to get a yield-stress fluid, and (iii) show that this has the potential as a generic methodology for the material-level design of other rheological properties.

2.2 Background

2.2.1 Design Process Theory

A generic design process follows six phases [13]: planning, concept development, system-level design, detail design, testing and refinement, and production ramp-up. The concept development phase – the focus of this paper – takes functional objectives and target specifications as inputs, and generates a multitude of possible product concepts which are then subject to selection and testing. In our work here, multiple material structure concepts are considered in order to achieve a particular rheology, a yield-stress fluid.

A design problem should be defined independent of the solution; the functional objectives and target specifications describe the desired *performance* of a product (or material). Defining the functional objective is a fundamental aspect of design and is the result of abstracting a problem to what is essential and general. An over-specified objective places creativity-stifling restrictions on the concept generation process leading to design fixation and thus less innovative technologies or materials [14]. However, a good functional objective also cannot be too broad in order to enable accurate framing and decomposition of the product's purpose as well as provide physical insight into how the design problem might be solved [15]. For the design of a yield-stress fluid, a poor functional requirement might be, "a polymeric network that flows under stress and reversibly solidifies at low stress". This mock-functional requirement is overly specific since it describes a particular material class, polymeric networks.

Once the functional objectives and target behavior have been established, generation of all possible product concepts can take place. This concept generation process separates into surveying existing concepts and creating new concepts. There are numerous handbooks and guides on how to approach creative concept generation; in general these approaches build upon

concepts from lateral thinking [16] including generating as many ideas as possible, going for quantity of ideas, and suspending negative judgement to a subsequent step in the evaluation process. The idea behind these approaches is to find as many different concepts as possible thus increasing the likelihood of identifying a great concept. Quite often these approaches can be seen as a waste of time by those inexperienced in effective design as they will only consider the first concept that is likely to provide a working design solution or concepts within their existing area of expertise rather than considering a more unfamiliar concept that may result in a vastly superior solution. Thus the danger in not creatively generating new concepts that may or may not result in producing the "best" design solution is that design fixation will occur as methods of problem solving become close-minded. Additionally, even should one of the first few promising concepts to be generated turn out to be "best", the generation of concepts beyond those does nothing to take away from the value of that initial concept. Rather, instead of a concept being chosen for being the only available option, it can be chosen as a concept that is obviously and justifiably superior to many other considered concepts [16].

Numerous techniques have been established for concept generation, such as free form or intuitive methods, structured methods, new perspectives techniques, and association techniques. In this paper we use a juxtaposition technique, combining two concepts to produce something new [16]. Systematic organization of the various existing and new concepts allows for a framework in which to synthesize and combine concepts or continue adding additional concepts. In a generic design process this systematic organization might take the form of a classification tree for a single function that facilitates comparison, or a combination table for combining different subfunctions [13]. Following a systematic concept generation process, concepts are

evaluated and a final concept or combination of concepts is selected. For the design of complex fluids concept evaluation involves material synthesis and rheological analysis.

When evaluating concepts an important aspect to consider is the degree of predictive capabilities available as predictive analysis greatly facilitates prototyping and testing the effectiveness of concepts [17]. Models allowing for predictive analysis are considered in this paper but the further downstream phases of the design process are not.

2.2.2 Materials Design Approaches

The general design processes of concept generation (surveying and creation) map in materials design to the categories of *material selection* and *material synthesis* as shown in Figure 2.2. When choosing what materials to incorporate into a product design, one can either select an existing concept or synthesize a new material. Oftentimes, selection is much simpler and cheaper but sacrifices significant freedom as the designer is limited to existing materials that have been characterized in the relevant ways.

For materials that are not rheologically complex, theories of material selection have been well developed. The most well-known materials selection method is described in [18]; a flowchart depicting this selection process is shown in Figure 2.3. The requirement for carrying out this process is a far-reaching and robustly organized database of material properties. Using this database, downselection occurs by considering application constraints and rankings of suitability. As stated, this process has found great success for simple materials, however the databases that the process is built upon are completely absent for rheologically complex materials. The closest approximations to such a database are rheological modifier handbooks [19,20], however these can be largely inadequate for design.

While rheological modifier handbooks do provide previous ways in which certain modifiers have been used, the already-limited lists of material properties that are necessary for downselection are lacking as the properties are provided for a particular percentage of additive and the function-valued nature of properties is not often addressed. As an example, though the immense importance of yield-stress fluids has already been stated, [19] and [20] each only mention the phenomenon once out of all the numerous rheological modifiers they list with only the former providing single viscosity values at particular weight percentages of additive.

Until relatively recently, the commonly held idea of materials synthesis has been mainly that of tailoring a particular (already selected) microstructure in order to mathematically optimize material properties using material process-structure and/or structure-property relations [21]. Examples of this approach can be found both for more traditional materials [22] and for rheologically complex materials [23]. While extremely useful in the downstream system-level and detail design phases, these studies have already assumed a particular microstructure type or chemistry to optimize and therefore have bypassed the concept development phase of the design process.

As mentioned, there is an increasing interest in using inverse methods in designing materials to achieve functional objectives [7,24] including a focus on properties which may be achieved by numerous formulations [12]. Until now these ideas have not been applied to rheologically complex material properties; by doing so here we hope to enable more creativity for these materials, in particular broadening the concept generation space before fixating on any particular structure.

2.2.3 Yield-Stress Fluids

Though it has been debated whether a "true" yield stress exists, yield-stress fluids have been accepted as a practical reality for most applications, with definitions hinging on the critical value of stress that must be reached. Example definitions include: "[a yield-stress fluid] does not flow if the imposed stress is below a threshold value, but it can flow rather easily after this value is exceeded [1]", and, "[a yield-stress fluid combines] solid-like behavior at low stresses with a fluid-like response at high stress [6]." The controversy over yield-stress fluids truly existing comes from the experimental observations of extremely slow flow even below any critical stress value [2], however on the timescales of many applications this deformation is not significant. Additionally, there are numerous ways in which a yield-stress may be characterized which are the focus of several reviews [3,25], however it is generally true that there is no sharp transition in flow behavior and thus "the yield stress" is actually representative of a relatively narrow range of stresses.

Shown in Figure 2.4 are two representations of apparent yield-stress fluid behavior based on steady shear flow characterization. The two equivalent representations, a plateauing shear stress as shear rate decreases (Figure 2.4a), and dramatic drop in viscosity across a narrow range of shear stress (Figure 2.4b), show the somewhat subjective nature of how one can report a precise value of the yield stress. For this paper, parallel disk steady flow is used, with corrected shear-stress values as a function of shear rate fit to the three-parameter Herschel-Bulkley model:

$$\sigma = \sigma_Y + K\dot{\gamma}^n \tag{2.1}$$

which we prefer to re-write as,

$$\sigma = \sigma_Y \left[1 + \left(\frac{\dot{\gamma}}{\dot{\gamma}_{critical}} \right)^n \right]. \tag{2.2}$$

To the knowledge of the authors, the representation of the Herschel-Bulkley model in Equation (2.2) has not been used before but results in the parameter $\dot{\gamma}_{critical}$ that is physically meaningful as a critical shear rate at which the flow stress is twice the value of the yield stress, σ_Y. This physical intuition is desirable compared to the parameter "*K*" which has units that depend on the parameter "*n*". Unless otherwise specified, reported values of a material's yield-stress were taken from the Herschel-Bulkley model fit but the widely used Bingham model was also fit for comparison. The two-parameter Bingham model which fits the yield stress and infinite shear viscosity, η_∞, is

$$\sigma = \sigma_Y + \eta_\infty \dot{\gamma}. \tag{2.3}$$

There have been attempts in the past to categorize yield-stress fluids based on the presence of a material restructuring time [26], and the microscopic mechanism by which the yield stress emerges for certain particulate systems [1], however none are from the perspective of design. This over-focus on analysis across a century of rheology literature has resulted in a scattered understanding of all the various ways to achieve a yield-stress fluid. Here we will bring together that scattered understanding and organize it into a useful paradigm for the design of yield-stress fluids, perhaps the most useful rheologically complex phenomenon.

2.3 Materials and Methods

The materials characterized for the start of this design database were well-studied *archetypal* yield-stress fluids, materials one may regard as "classic" yield-stress fluids within rheological literature. Refer to Table 2.1 for the specific material formulations presented in this paper. Carbopol 940 obtained from Acros Organics was mixed in distilled water for thirty

minutes before being neutralized to a pH of 7 using a sodium hydroxide solution, resulting in swollen microgel particles that pack together at sufficiently high concentrations [27]. Silicone oil-in-water emulsions were synthesized with 1000 cSt (at 25 °C) silicone oil obtained from Sigma-Aldrich and deionized water; sodium dodecyl sulfate from Fisher Scientific was used as the emulsifier. The mixture was homogenized at 5000rpm for 10 minutes using an IKA T-18 homogenizer with a S18N-19G attachment. Mineral oil-in-water emulsions were synthesized by the same procedure using light mineral oil from Sigma Aldrich which has a viscosity of between 14.2 and 17.0 cSt at 40 °C. Bentonite from Sigma Aldrich was dispersed in steam distilled water using an overhead stirrer at approximately 300 rpm until mixed, at which point the clay particles form a percolated gel network [26]. The Laponite RD suspension which also has particles which can attractively interact, was synthesized by the same procedure as Bentonite with powder obtained from Conservation Support Systems. Xanthan gum from *Xanthomonas Campestris*, a polymer which is known to form structure in solution through self-associative intermolecular attractions [28], was obtained from Sigma-Aldrich; solutions were synthesized by slowly adding xanthan gum powder to deionized water being mixed with an overhead stirrer at between 300 and 600 rpm, continuing to mix for 5 minutes after which the mixture was covered with tin foil and placed on a hotplate at 80 °C to mix at 400 rpm for 30 minutes.

Rheological characterization was performed on a TA Instruments DHR-3 or AR-G2 rotational rheometer (combined motor/transducer instruments) using a parallel-plate geometry with a diameter of 40 millimeters. Depending on the sample, either a sandblasted plate, 600 grit or 60 grit adhesive-backed sandpaper was used to prevent slip. Materials were tested at multiple gaps to verify the absence of slip [29]. Parallel-plate corrections were used to identify the true shear stress. Apparent stress, σ_A, values were fit to a polynomial curve and corrected using,

$$\sigma_{True} = \frac{\sigma_A}{4}\left[3 + \frac{d\ln\sigma_A}{d\ln\dot{\gamma}_{True}}\right], \tag{2.4}$$

where $\dot{\gamma}_{True}$ is the applied shear rate [30]. Unless otherwise specified, all tests are performed from high-to-low shear rates, thus the yield stress is a dynamic yield stress rather than a static yield stress [26]. For some materials, especially at smaller gaps, an increasing stress was observed at lower shear rates (Figure 2.5B, Appendix Figure 1). In the case of these materials, the Herschel-Bulkley model was only fit from the higher shear rates corresponding to the highest and lowest values of corrected stress. When fitting the Bingham model, for all materials the yield-stress parameter was constrained to the lowest corrected stress value. All fitting was performed with variance weighting using OriginPro 9.0 software.

2.4 Results

2.4.1 Rheology-to-Structure Inverse Problem and Organization

The evidence that designing a yield-stress fluid is an inverse problem at all, that there are numerous possible ways to achieve the same yield stress, can be seen in Figure 2.5. For three materials with different chemistry and microstructure, approximately the same yield-stress (indicated by the dashed lines) can be achieved by varying the weight-percent of the additive in each case. For the highlighted curves of A) Carbopol, B) Laponite, and C) a silicone oil-in-water emulsion, the fit yield stress parameters are σ_Y = 29.6, 35.4, and 24.4 Pa respectively. Given that the yield stress value identifies a narrow range of stress over which the material's viscosity changes, the differences between these three values is unlikely to make a difference in all but the most precisely demanding applications. While the three yield stresses are essentially the same, additional material properties can vary considerably and will be discussed later (high-rate

viscosity, critical shear rate, etc.). Therefore, since these differing materials are able to achieve the same value of what is likely to be one's primary design objective, the yield stress, one should consider all the material options available and use secondary design objectives or properties as the criteria to motivate creative material designs.

In order to facilitate more useful design practices for yield-stress fluids and rheologically complex materials in general, the organization of the discipline must be the inverse of that shown in Figure 2.1. Rather than only targeting a particular microstructure for exhaustive characterization, a property-based organization as shown in Figure 2.6 must be adopted; particular properties are targeted and all possible ways of achieving that property must be determined.

A likely reason why the field of rheology has not been organized based on properties to date is because of the way in which many rheologically complex properties differ from typical properties in simpler solid materials; while every metal has a strength, linear elastic modulus, etc., not every complex fluid has a yield stress, for example. The key to exhaustively determining the possible ways in which a particular rheologically complex property might be achieved is by adopting an appropriate functional objective, one that provides physical insight into the mechanism by which a property comes about. As they are focused on the analysis point of view, the premier review articles and texts on yield-stress fluids do not state what would essentially be a functional objective in a way that is adequate for design.

The closest statement to a functional objective would be the definitions that these review articles present; quoted earlier in Section II, these definitions provide only a superficial description of yield-stress fluids with no insight into how one might achieve such a material. If given a phenomenological definition such as, "[a material] that shows little or no deformation up

to a certain level of stress [and] above this yield stress the material flows readily [30]", one would be exceptionally unlikely to successfully ideate new materials satisfying that definition and would instead be limited to pre-existing lists of example materials which as discussed in Section II are themselves sorely lacking. In this way, the existing functional objectives are limiting since they are not expressed in a way that allows one to think completely independently of existing solutions/materials.

Here, for yield-stress fluids we propose the following functional objective:

A yield-stress fluid is able to bear a static load for long timescales (high viscosity at low stress) with shear-reversible mechanical connectivity (dramatic drop in viscosity above the yield stress) that is recoverable.

While somewhat long-winded in order to avoid the debated low-stress behavior, this newly proposed functional objective provides physical insight into how one might achieve a yield-stress fluid in a precise way that is both formulation- and structure-agnostic so as to not overly constrain the concept generation process. Rather than attempting to invent a way for viscosity to transition across multiple orders of magnitude, a designer can instead use intuition and experience about methods of bearing static loads that are able to reform after mechanical disruption.

For existing yield-stress fluids, there are two known mechanical interactions by which our proposed functional objective is satisfied: (i) jammed, repulsive interactions; and (ii) networked, attractive interactions. While these concepts of arrested structures have been well developed as "glasses" and "gels" respectively [31–34], they have never been used to organize yield-stress fluids and provide insight into how they might be designed and how different material systems might differ or be similar in their properties and behavioral trends.

Figure 2.7 organizes representative yield-stress fluids based on the two mechanisms of jammed versus networked microstructures. Materials where a static load is borne primarily by the microstructure jamming, eventually yielding once the structure is able to rearrange and slide past itself, have been termed "repulsion-dominated". Examples within this group include microgel suspensions such as Carbopol, oil-in-water emulsions, and foams which are pictured. Additional materials known to exhibit a yield-stress that are repulsion-dominated are spherical micellar solutions, and suspensions of hard and charged-particles. Though the chemistry varies wildly within and across these material classes, the yield-stress comes about through the same physical mechanism of repulsive interactions; as seen in the images in Figure 2.7, morphologically these material classes are very similar. Materials where a static load is borne primarily by the microstructure resisting being pulled apart, eventually yielding once these re-formable attractions have been broken have been termed "attraction-dominated". Examples within this group include particulate gels such as Bentonite, magneto- and electro-rheological fluids, and fibrillar or polymer solutions that have physical crosslinks and therefore can re-form. Within this group, the morphological similarity is that of a sparse percolated network spanning the sample that must be destroyed for yielded flow to occur. For both of these groups the "-dominated" qualifier has been used to acknowledge combinations of both mechanisms, such as attractive glasses [31]. Note that both the repulsion-dominated and attraction-dominated categories are capable of including materials that may have very similar ingredients. For instance, colloidal suspensions can exist as either glasses or gels. Thus this structural organization transcends the traditional academic organization by ingredient such as by "particle" or "polymer" [5].

With our proposed functional objective and the resulting classification tree, the material design methodologies of selection and synthesis for yield-stress fluids are both greatly facilitated. Selection strategies benefit by being able to effectively generate lists of existing candidate materials to choose from, as well as insights into the comparative relations between material classes. With an adequate functional objective, creative synthesis based on physical insight can occur, with the classification tree allowing for structured concept generation.

2.4.2 Yield Stress Scaling Behavior

As mentioned in Section II, in material *synthesis* structure-property relations are important to consider as tools for predictive analysis. The full scientific understanding of all material structures currently known to produce a yield-stress is underdeveloped due to the complexity of calculating macroscopic properties from the underlying microstructure and molecular features. In contrast to complex fluids, developed areas of mechanical design have very clear mathematical models to represent system behavior (e.g. linkage dynamics). A unique aspect with material synthesis for rheological properties is that governing equations are not always known. In the specific case of yield-stress fluids, if any predictive equations are available, they are often scaling laws that relate the yield stress to underlying structure. Available scaling laws for yield-stress fluids are collected in Table 2.2. This table is useful in the evaluation of concepts since the presence of these predictive equations is greatly advantageous as they can demonstrate the feasibility of a concept to achieve a particular performance; between two otherwise comparable concepts, one would prefer a concept with a readily available predictive scaling law. While not the focus of this paper, these scaling laws would be eminently useful further downstream in the design process when attempting to determine final formulations in the system-level and detail design phases.

Most of the presented structure-rheology scaling relationships involve the volume fraction of some dispersed phase of the material, however oftentimes in formulation it is much easier to control the weight-percentage of an additive rather than its volume. Being a very well-studied material system, Carbopol 940 has specific scaling equations relating the weight-percentage additive, C, directly to the yield stress for two different concentration regimes [27],

$$\sigma_Y = \left(\frac{C}{0.0335} - 1 \right)^3 \tag{2.13}$$

$$\sigma_Y = 45 \left(\frac{C}{0.124} \right)^{1/3}. \tag{2.14}$$

These correlation formulas agree reasonably well with our experimental results for Carbopol seen in Figure 2.8 alongside the other tested material systems. The weight-percentage of additive is often of great importance when designing a completely new material or modifying an existing material to give it a yield stress. Typically a low percentage of additive is desirable since it will be less likely to modify other properties such as flavor and texture, and obviously less additive is often less costly. Based on the classification tree of yield-stress fluids we can see that the networked, attractive systems achieve yield stresses at moderate values of weight-percentage, while the jammed, repulsive emulsions require a significant percentage of added-oil for comparable yield stress values. The swollen nature of the Carbopol microgels are what result in such a low weight-percentage of additive giving rise to a jammed yield-stress fluid and is the reason that Carbopol is considered a “high-efficiency” rheological modifier [19]. Obviously there are endless parameters and material properties that might be crucial for one’s application such as transparency and other optical properties, conductivity, biocompatibility, and biodegradability. In the next section, we will compare parameters that are representational of the

steady flow behavior to enable the application of material selection principles to function-valued properties.

2.4.3 Low-Dimensional Descriptions for Selection of Yield-Stress Fluids

For selection, as discussed, the material property databases that are foundational for other types of materials design are simply not present for rheologically-complex materials, hindered in their creation by the fact that not all materials will have all properties. Rather than needing to laboriously characterize the hundreds of entries in a rheological modifiers handbook, one can instead consider if the modifier might possibly satisfy the functional objective and only characterize those expected to have a yield stress. While mistakes will most certainly be made in this process, e.g. materials anticipated to have a yield stress will show no such signature or materials that do have a yield stress may be overlooked, it will be far less onerous and implausible than characterizing every possible ingredient hoping to see a particular signature.

Once materials databases are more effectively generated, the classification tree of yield-stress fluids can provide one with insight into how and why the behavior of particular materials and classes of materials relate or differ when compared. Since a particular value of yield stress can be achieved by multiple materials, applying additional design constraints on secondary parameters or properties is a critical step in converging on a final design choice in a rational, non-arbitrary way. However, due to the function-valued nature of the rheologically-complex material properties, low-dimensional representations are necessary for their easy comparison. Information is always lost when representing complicated data in a low-dimensional way, here we will consider different models which communicate information to varying degrees of completeness, and discuss the situations in which the loss of information can be appropriate.

Shown in Figure 2.9 are three possible low-dimensional descriptions of a the steady flow behavior of a yield-stress fluid: two values of shear stress (the yield-stress parameter from the Herschel-Bulkley model and the stress at a reference shear rate); the two-parameter Bingham model, Equation (2.3); and the three-parameter Herschel-Bulkley model, Equation (2.2). Clearly the reference-shear-rate representation loses a significant amount of information about the flow curve, however depending on one's needs it could be perfectly adequate and has been used when selecting for minimum rheological criteria [5]. The two-parameter Bingham representation in most cases can do a reasonable job of capturing the yield stress and the high shear-rate viscosity and has been useful as allowing for the simplest model interpretation [35]. However, the Bingham model can completely miss information regarding intermediate shear rates, and so in most cases for an accurate representation of the entire flow-curve a model with more parameters such as the Herschel-Bulkley is necessary; this of course comes at the cost of added complexity (higher-dimensional co-plots) and may result in decreased physical meaning. In the case of the use of Equation (2.2), this is limited to issues in the interpretation of parameter "*n*" which most loosely interpret as the degree to which a material shear-thickens for $n > 1$ or shear-thins for $n < 1$.

Depending on one's design constraints, one representational comparison might be more or less useful than another. For example, if one knows that their final design will be restricted to a particular shear rate and they are unconcerned with any other aspect of the flow behavior, then it would be most useful to choose from the Ashby style plots of the 'reference shear rate' representation at three different shear rates shown in Figure 2.10 rather than from full-curve representations which would add needless complexity. Within these plots, the particular shear rate of an application design will further dictate the usefulness of such a comparison. As seen in

Figure 2.10A, at the lowest shear rate of 0.01 s^{-1}, materials are not differentiated in any way as they all have yet to deviate significantly from the yield stress value; in terms of this shear-rate design constraint, any choice of material is as good as any other choice, however this is not the case for the other, higher shear rates.

For the higher reference shear rates (Figure 2.10B-C), we begin to see differentiating behavior of the flow stress based on the classification tree of design strategies. This differentiation is most clear in Figure 2.10B where the oil-in-water emulsions and Carbopol (material systems where the yield-stress comes about due to jamming) have higher flow stresses than either of the two particulate gel samples. In Figure 2.10C, at the highest measured shear rate it is notable that while all other materials including Bentonite have increased from the yield value, the shear stress of the other particulate gel, Laponite, still has not increased appreciably. This effect could also be seen in Figure 2.5B, where Laponite has an extremely flat flow curve. This differentiating behavior of Laponite and Bentonite also manifests itself in the other low-dimensional representations: Bingham and Herschel-Bulkley model descriptions.

Shown in Figure 2.11 is the comparative plot of the parameters from the Bingham model fit, the simplest whole-curve representation of a yield-stress fluid. While not as accurate a fit as the Herschel-Bulkley model as evidenced by the visual deviation from the data seen in Figure 2.9, important insights into designing new materials and into the high-rate viscosity can be obtained from the comparison of these Bingham model parameters The insights for design of materials come from the scaling behavior of parameters for different material types and the regions which they inhabit within the parameter space. Until such time as every yield-stress fluid one could possibly want has already been made and characterized, people will always need to try to expand the performance limits of materials and the scaling behaviors and inhabited regions

give an idea of what one can expect. For example, in Figure 2.11 both of the oil-in-water emulsions show the interesting scaling behavior of the infinite shear viscosity, η_∞, being nearly flat, varying by less than half an order of magnitude, across one-and-a-half orders of magnitude in yield stress, σ_Y. Therefore, one can expect that if one wanted to try and modify a material with an increased yield stress without substantially increasing the high-shear-rate viscosity, an oil-in-water emulsion would be one possible candidate for doing so. Similarly, due to the region they inhabit, one can infer that generally particulate gel systems will have the lowest viscosities at high shear rates.

A more complete fit of the data results from the three-parameter Herschel-Bulkley model, parameters shown in Figure 2.12. The added complexity of this representation is immediately apparent in that three separate comparative plot projections are necessary to see the full relationships of representations. In some cases, it is unclear if any meaningful relation can be determined such as in the plot of "*n*" versus critical shear rate seen in Figure 2.12C, where the parameter curves of several materials bend back around on themselves significantly. However, we are still afforded great insight into how the materials will behave across all shear rates from Figures 2.13A and 2.13B without needing to see the material flow curves at all, and this with just a three-parameter fit.

Starting with Figure 2.12A, the critical shear rate, $\dot{\gamma}_{crit}$, allows us to determine when the flow stress will begin to deviate from the yield stress by a factor of one-hundred percent. The range of critical shear rates observed is approximately $0.2 \leq \dot{\gamma}_{crit} \leq 3000$ s^{-1} with oil-in-water emulsions having very low values of critical shear rate, followed next by Carbopol, then by the particulate gel systems. Comparing this to Figure 2.9, at the lowest shear rate of 0.01 s^{-1} (Figure

2.9A), below our observed range of critical shear rates, no materials have deviated from the yield stress, exactly as we would expect. Based on Figure 2.12A, at 10 s^{-1}, the materials we can expect to have deviated from their yield stress are the oil-in-water emulsions, Carbopol, and the lowest weight percentage of Bentonite. Comparing to Figure 2.10B this is exactly what we see, with only most of the Bentonite samples and Laponite still very close to their yield stress. In Figure 2.12A at 100 s^{-1} we expect the stresses of almost all of the Bentonite samples to have increased significantly, with Laponite yet to do so; again this is in agreement with Figure 2.10C.

Using Figure 2.12B, one can also anticipate even more features of Figure 2.10C such as the significant increase in Bentonite's stress from Figure 2.10B compared to Carbopol. As seen in Figure 2.12B, all the Bentonite samples have values of "*n*" that are significantly higher than the Carbopol samples. According to Equation (2.2), what this means is that while the Bentonite flow curves are flatter than the Carbopol flow curves for $\dot{\gamma} < \dot{\gamma}_{crit}$, above $\dot{\gamma}_{crit}$ the Bentonite flow stresses will increase significantly faster than Carbopol. Additionally, Figure 2.12B showcases differentiation of the materials correlating with the classification tree (Figure 2.7) with systems with networked attractions having higher values of "*n*" that vary significantly with the yield stress, while the repulsive jammed systems have lower values of "*n*" that are much flatter as the yield stress is varied. Thus taken together, Figures 2.12A and 2.12B allow one to make general qualitative comparative statements on the behavior of the various material classes such as that the networked systems will increase in stress much more strongly than the jammed systems, but that the jammed systems will typically deviate from their yield stress earlier (excepting xanthan gum). It is important to note that these comparisons with the Herschel-Bulkley model are only possible due to our re-write of the model seen in Equation (2.2); the parameter "K" in the traditional Herschel-Bulkley model (Equation (2.1)) cannot be used in comparative co-plots as

"K" changes units as a function of the "n" parameter. All of this comes in addition to being able to accurately reproduce the complete flow-curve if ones application dictates it since all the necessary parameters are specified compactly.

2.4.4 Synthesis Approaches for Yield-Stress Fluids

In addition to the physical insight afforded by our functional objective which is crucial to successfully ideate new material concepts, the classification tree allows for the structured generation of a framework in which to ideate these concepts and to intuit existing materials. Here we present one possible concept generation strategy; a vision for the future design of yield-stress fluids. Shown in Figure 2.13 is a visualization of a juxtaposition concept generation process between material microstructures to achieve a yield stress. This organizational framework is for the combinations of two individual material classes with representative classes pictured. Here the general state of knowledge for each entry is indicated in the matrix. Each entry will be referred to using "(row, column)" notation with each grey square representing an individual material class using the same A-F notation as in Figure 2.7. Covered are currently known materials as well as new possibilities for materials; combinations of primary structures exist off-diagonal, and might be an existing material that has been studied as in the case of a mixture of a magnetorheological fluid and fibrillar gel (grease) [36], or material structures that have never been described in the open literature. Of course, any particular combination is subject to the constraints of chemical compatibility or the ability to actually synthesize the material. Additionally, just as in mechanical design, a conceptual combination in no way assures that the functional specifications will be met, but does broaden the available possibilities. Though many of the presented juxtapositions at first glance may not necessarily suggest any additional benefit over others, this method is a quick and simple way of generating a very large number of possible ideas. Many combinations are being

studied because they are in fact scientifically interesting, have novel properties, or both. For example, a combination of particulates and emulsion droplets as pictures in (A,B) are being investigated in the form of bimodal dispersions of starch and fat droplets [37]. Microgels made field-responsive would correspond to (A,E) [38]. Entry (C,D) applies to whipped cream which can be conceptualized as a foam stabilized by a particulate gel network [39]. Composite microstructures appearing very recently in scientific literature include photocrosslinkable nanoemulsions which creates a sparse network of emulsified droplets represented by (B,D) [40], and nanoparticle solutions used as an adhesive between polymer gels [41] which is not pictured but can be conceptualized as a composite of particulate and polymer gels. Other composite materials not pictured include field-responsive polymer gels [38], and yogurt which is a combination of a polymer gel and an emulsion [39]. Of course, in juxtaposition, one is not limited to combining only two yield-stress fluid concepts to result in a new yield-stress fluid. One could combine any number of concepts, or perhaps combine a yield-stress fluid concept with a structure that would have no yield stress. For example, a schematic is shown in Figure 2.13 for a concept that has not yet been investigated in open literature, a combination of an emulsion which is a yield-stress fluid with an interstitial transient network which would provide no yield stress but could perhaps modify other desirable properties.

2.5 Conclusions

Here we have presented a new paradigm of yield-stress fluids which is useful from a design perspective. This organization based on the underlying structural mechanism by which the yield-stress comes about was the result of applying principles of designing via inverse methods in order to define an effective functional objective which is formulation- and structure-

agnostic. Our proposed organization provided insight into concept evaluation through the comparison of low-dimensional models for yield-stress fluid flow behavior, allowing for qualitative comparisons between material classes depending on the structural mechanism of their yield stress. The evaluation as a comparative tool of the model considered here which preserved the most information regarding the complicated flow data, the Herschel-Bulkley model, was enabled through our new representation of the model seen in Equation (2.2).

As discussed, yield-stress fluids are the most used and perhaps the most useful rheologically-complex materials. Here, for yield-stress fluids we have provided a methodology and insights for broadening the available design space, and the evaluation of design concepts based on available predictive analysis and the comparison of simply represented flow data. Anyone wishing to utilize yield-stress fluids in some product or application should follow the methods presented here, making use of our early-stage database and more importantly considering all possible concepts rather than blindly accepting the most obvious approach.

The design-space presented here is obviously incomplete. Not all materials and microstructure types that produce a yield-stress fluid are known by the authors or by anyone else. However, by following the functional objective proposed here, significant progress can be made on effectively deciding what materials are capable of producing a yield-stress fluid to then be evaluated and characterized appropriately. These same methods of design must also be applied to other rheological phenomena (e.g. linear viscoelasticity) which are currently under-utilized. Everything presented here has only been to relate a particular rheology, the yield-stress, to numerous structures, the latter stage of the "Design of Materials" schematic outlined in Figure 2.1. To effectively design complex materials in the future will mean completely integrating methods of relating complex performance and behavior to numerous candidate rheological

phenomena, and then finally to even more multitudes of structures/formulations. The full design process includes making a choice of material and then attempting to optimize the specific formulation and structure (through iteration or other means); the synthesized material must first be validated to ensure that the property of interest has been achieved, and then validated further for performance in the actual application of interest.

2.6 Figures and Tables

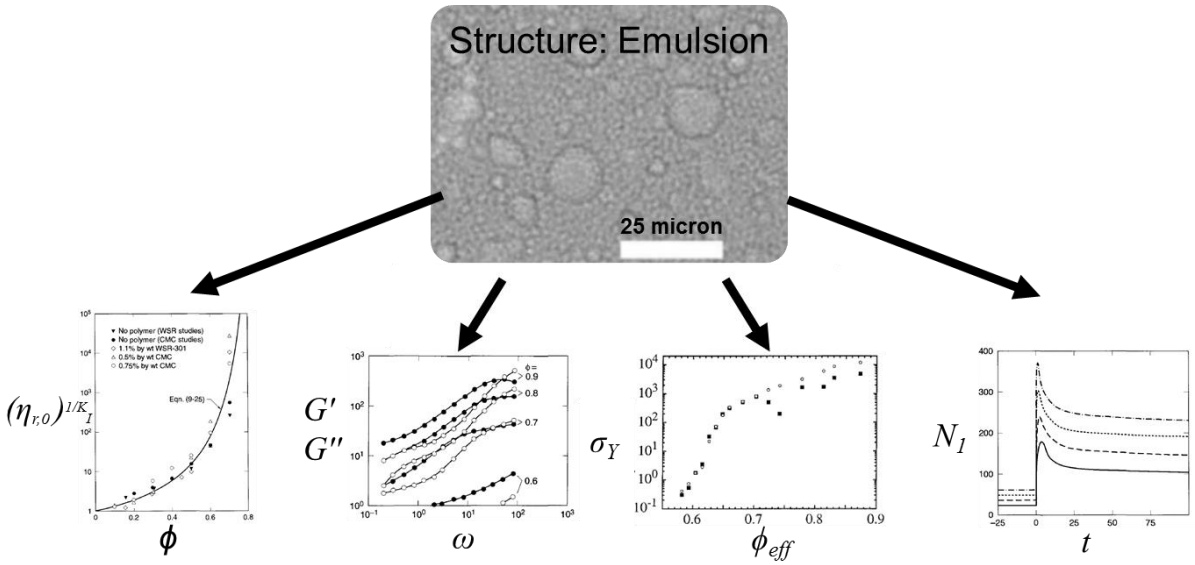

Figure 2.1. The analysis approach: single material structure, multiple properties. As an example, an emulsion (image from [42]) has multiple rheological properties (plots from left-to-right from [43–46], respectively). Organization in this manner (for instance in [47]) is a composition focused grouping; design requires the inverse method of grouping by property. $\eta_{r,0}$ is the zero-shear relative viscosity, K_I is given by [43], ϕ is the droplet concentration, G' and G'' are the storage and loss modulus respectively in Pascals, ω is frequency in inverse seconds, σ_Y is the yield stress in dynes/cm^2, ϕ_{eff} is the effective volume fraction, N_1 is the first normal stress difference in Pascals, t is time in seconds.

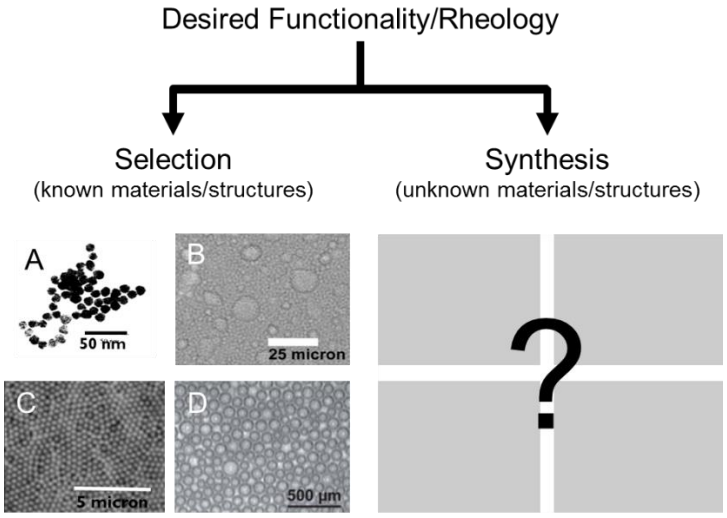

Figure 2.2. To design is to make decisions, either by *selection* or *synthesis* of materials. The arrows emphasize these two possibilities in the rheology-to-structure inverse problem. Images show examples of known materials that may behave as yield-stress fluids; (A) particulate gel from [48], (B) emulsion with high volume fraction dispersed phase from [42], (C) microgel suspension from [49], (D) foam from [50].

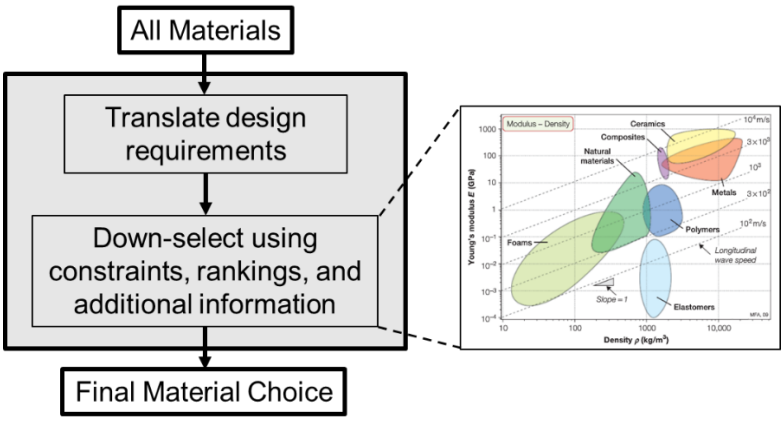

Figure 2.3. Material selection method (adapted from [18]). Starting from a database of all surveyed materials, design constraints and further research enable one to down-select to a final material choice. A common tool used in the down-selection process is the "Ashby diagram" (pictured from [18]) which is a material-property co-plot used to compare and show trends of multiple material properties within different material types.

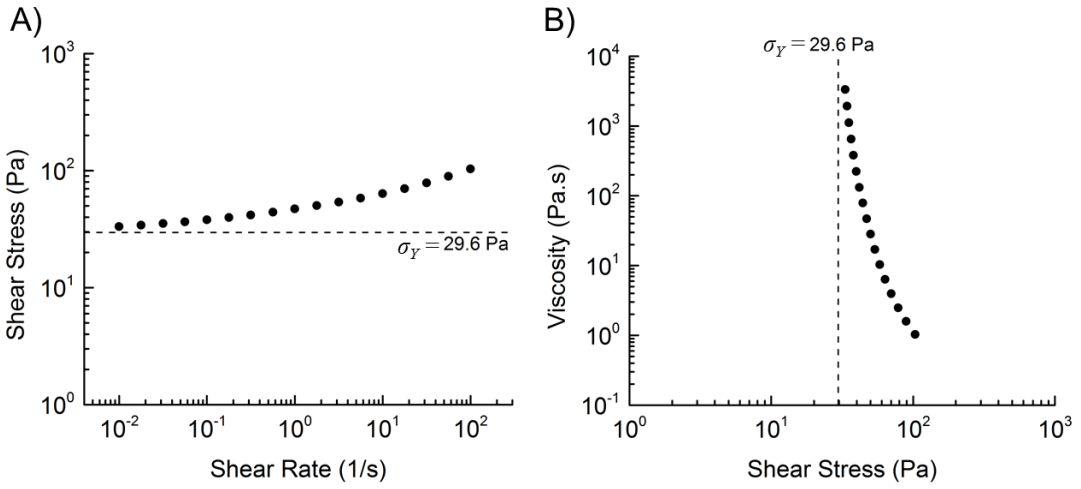

Figure 2.4. Two representations of apparent yield-stress fluid behavior; steady flow shear stress, σ, for 0.15% Carbopol, measured with decreasing shear rate, $\dot{\gamma}$. An apparent yield stress is indicated by (A) a stress plateau over a wide range of shear rate, or alternatively (B) a dramatic drop in viscosity, $\eta \equiv {}^{\sigma}/_{\dot{\gamma}}$, occurring over a narrow range of stress. The apparent yield-stress can be subjective regarding the approach one takes to determine it. For this paper the parallel-plate corrected shear-stress values were fit to a Herschel-Bulkley model, Equation (2.2), to determine the yield-stress parameter, σ_Y .

Table 2.1. All presented material formulations organized by material and weight-percentage of additive. For specific synthesis procedure refer to Section 2.3 Materials and Methods.

Material	Formulation
Carbopol	Specified weight-percentage of Carbopol 940 in distilled water, neutralized to pH 7 with sodium hydroxide
0.1%wt	
0.15%wt	
0.2%wt	
0.25%wt	
0.5%wt	
Silicone Oil-in-Water Emulsion	
65%wt	65wt% silicone oil, 23.33wt% deionized water, 11.67% sodium dodecyl sulfate
70%wt	70wt% silicone oil, 20wt% deionized water, 10wt% sodium dodecyl sulfate
75%wt	75wt% silicone oil, 16.67wt% deionized water, 8.33wt% sodium dodecyl sulfate
80%wt	80wt% silicone oil, 13.33wt% deionized water, 6.67wt% sodium dodecyl sulfate
Mineral Oil-in-Water Emulsion	
65%wt	65wt% mineral oil, 23.33wt% deionized water, 11.67% sodium dodecyl sulfate
75%wt	75wt% silicone oil, 16.67wt% deionized water, 8.33wt% sodium dodecyl sulfate
Bentonite	Specified weight-percentage of Bentonite in distilled water
7%wt	
8%wt	
9%wt	
10%wt	
11%wt	
12%wt	
Laponite	Specified weight-percentage of Laponite RD in distilled water
3.5%wt	
4%wt	
5%wt	
Xanthan Gum	Specified weight-percentage of xanthan gum from *Xanthomonas Campestris* in deionized water
2%wt	
4%wt	
5%wt	

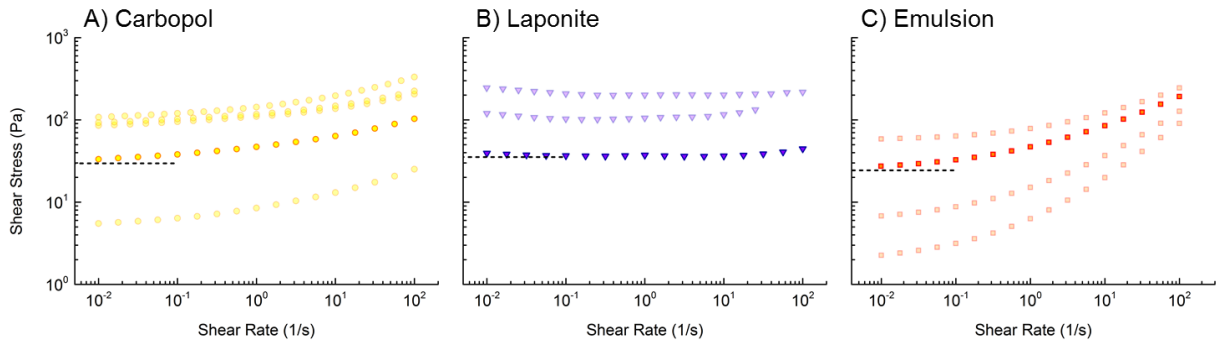

Figure 2.5. Steady simple shear flow from high to low rate for three differently structured materials. (A) Carbopol of 0.1, 0.15, 0.2, 0.25, 0.5 %wt; (B) Laponite of 3.5, 4, 5 %wt; (C) silicone oil-in-water emulsion of 65, 70, 75, 80 %wt of oil. In all cases a higher concentration increases the yield stress. The highlighted curves (bold symbols) shows that all three materials can have approximately the same yield-stress (shown as a dashed line for each material). Constraints on secondary properties or property scalings will determine suitability for design requirements.

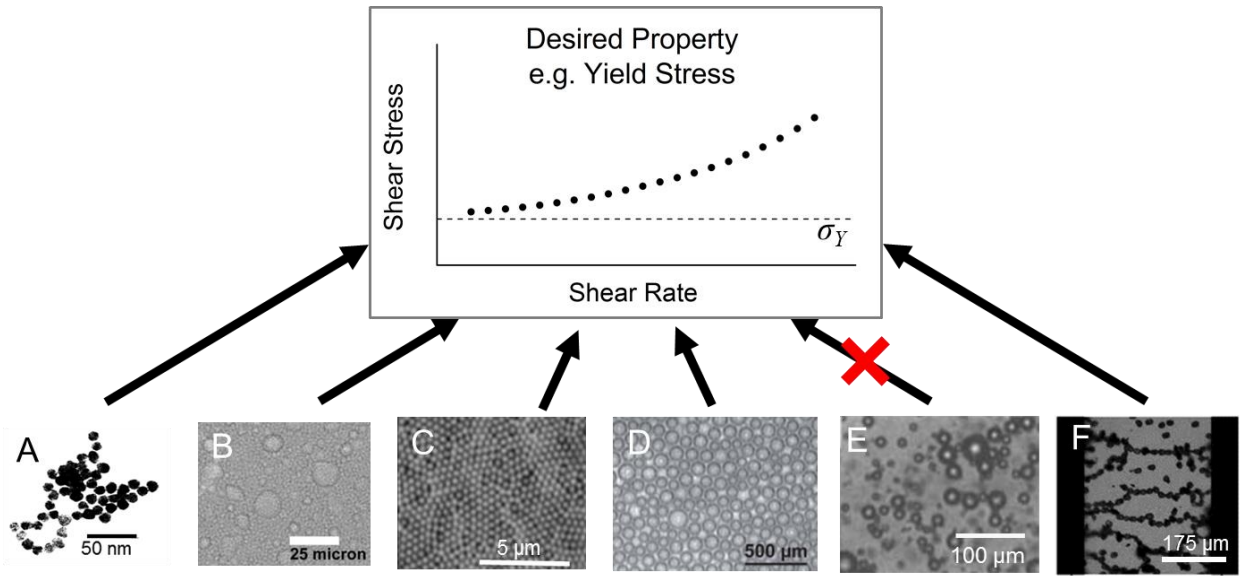

Figure 2.6. The design approach of materials science: a particular material property is targeted and all possible microstructures capable of producing that property are considered. Shown here, A) particulate gel [48], B) emulsion [42], C) microgel suspension [49], D) foam [50], and F) electrorheological fluid [51] are all capable of producing a material with a yield stress. Some materials such as E) an emulsion with a low enough volume-fraction of dispersed droplets do not have a yield stress [52].

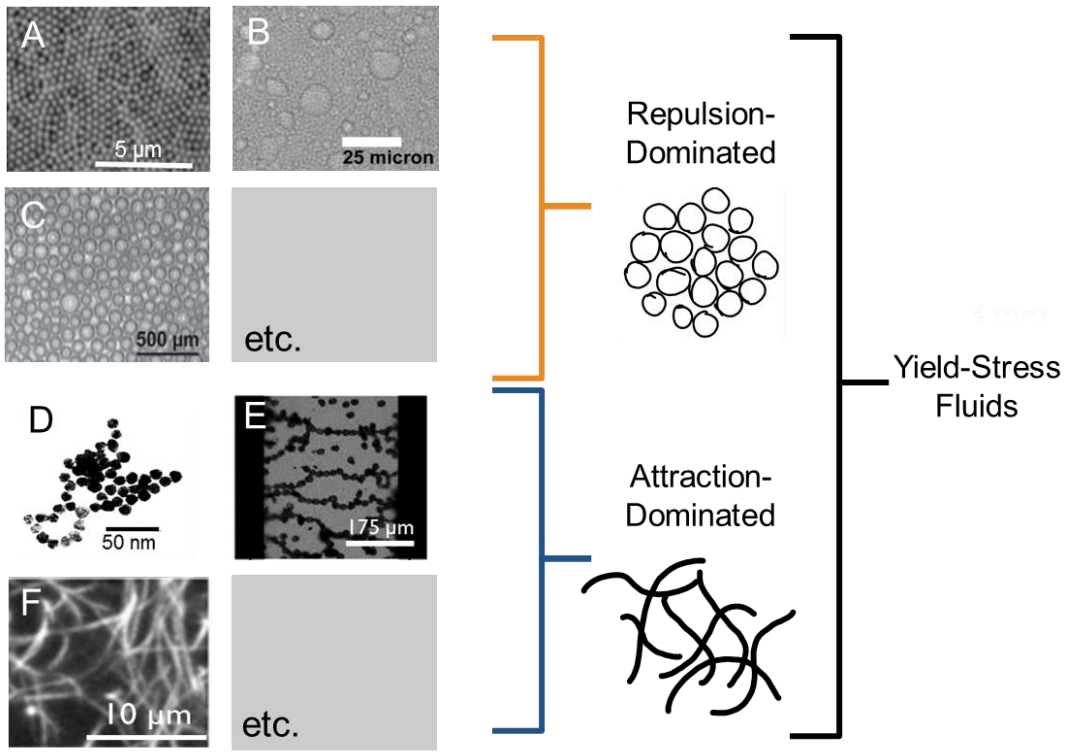

Figure 2.7. Concept generation, for existing and potentially new materials, is aided by organizing design strategies. For yield-stress fluid design, two generic strategies can be grouped as 'repulsion-dominated' and 'attraction-dominated' (although combinations also exist, e.g. attractive glasses). Examples shown are (A) particulate suspensions [49], (B) emulsions [42], (C) foams [50], (D) particulate gels [48], (E) electro/magneto-rheological fluids [51], and (F) fiber gels [53].

Table 2.2. Structure-rheology scaling relationships and equations for yield-stress fluid material classes. These relationships are useful for concept evaluation and synthesis as they allow one to predict the resulting yield-stress to varying degrees. See Table 3 for the definitions of all variables.

Material Class	Yield Stress Scaling Relationship	Notes	Reference
Particulate Suspensions			
Hard Spheres	$\sigma_Y = \sigma_{Crit} + 112\sqrt{\phi - \phi_{Crit}}$ (2.5)	$\phi > \phi_{Crit}$	[54]
Charged Particles	$\sigma_Y \approx K\left(\frac{W(r_m) - k_B T}{(r_m/2)^3}\right)$ (2.6)	$r_m < d_{eff}$ $K = constant$	[55]
Soft Particles	See Reference		[56]
Emulsions and Foams	$\sigma_Y = \frac{\Gamma}{R_{mean}}\phi^{\frac{1}{3}}Y(\phi)$ (2.7)	$\phi > 0.9069$	[57]
Particulate Gels	$\sigma_Y \sim \frac{\phi^2}{a^2}W'_{\max}$ (2.8)	$\phi < 0.64$	[58]
Electrorheological Fluids	$\sigma_Y \sim \phi\varepsilon_0\varepsilon_S\beta^2E^2f_m$ (2.9)		[59]
Magnetorheological Fluids	$\sigma_Y \sim H^2$ (2.10) $\sigma_Y = \sqrt{6}\phi\mu_0 M_S^{\frac{1}{2}}H^{\frac{3}{2}}$ (2.11) $\sigma_Y^{Sat} = 0.086\phi\mu_0 M_S^2$ (2.12)	Low field strength Intermediate field strength Fully-saturated yield strength	[60]
Polymer Gels	-		
Fibrillar Gels	-		

Table 2.3. Variable definitions for yield stress scaling relationships. Note: *F* indicates units of force, *L* indicates units of length, *A* indicates units of electrical current, *t* indicates units of time.

Variable	Definition
$\phi_{Crit} \doteq [-]$	Critical volume fraction for yield stress scaling to apply
$\sigma_{Crit} \doteq \left[\frac{F}{L^2}\right]$	Yield stress at critical volume fraction
$W(r_m) \doteq [FL]$	Interaction potential at average interparticle separation
$d_{eff} \doteq [L]$	Effective diameter of particle, where $W(r = d_{eff}) \approx k_B T$
$\Gamma \doteq [F / L]$	Surface tension
$R_{mean} \doteq [L]$	Sauter mean radius, $R_{mean} = 3\frac{Volume}{Surface\ Area}$
$Y(\phi) \doteq [-]$	Scaled contribution per drop to yield stress, $Y(\phi) = -0.08 - 0.114\log(1-\phi)$
$a \doteq [L]$	Particle radius
$W'_{\max} \doteq [F]$	Maximum spatial gradient of interaction potential
$\varepsilon_0 \doteq \left[\frac{(At)^2}{FL}\right]$	Permittivity of space
$\varepsilon_S \doteq [-]$	Relative permittivity of solvent
$\beta \doteq [-]$	Effective polarizability of particle
$E \doteq \left[\frac{F}{At}\right]$	Electric field strength
$f_{\max} \doteq [-]$	Maximum dimensionless restoring force between particles
$H \doteq \left[\frac{A}{L}\right]$	Magnetic field strength
$M_S \doteq \left[\frac{A}{L}\right]$	Saturated magnetic field strength
$\mu_0 \doteq \left[\frac{F}{A^2}\right]$	Permeability of space

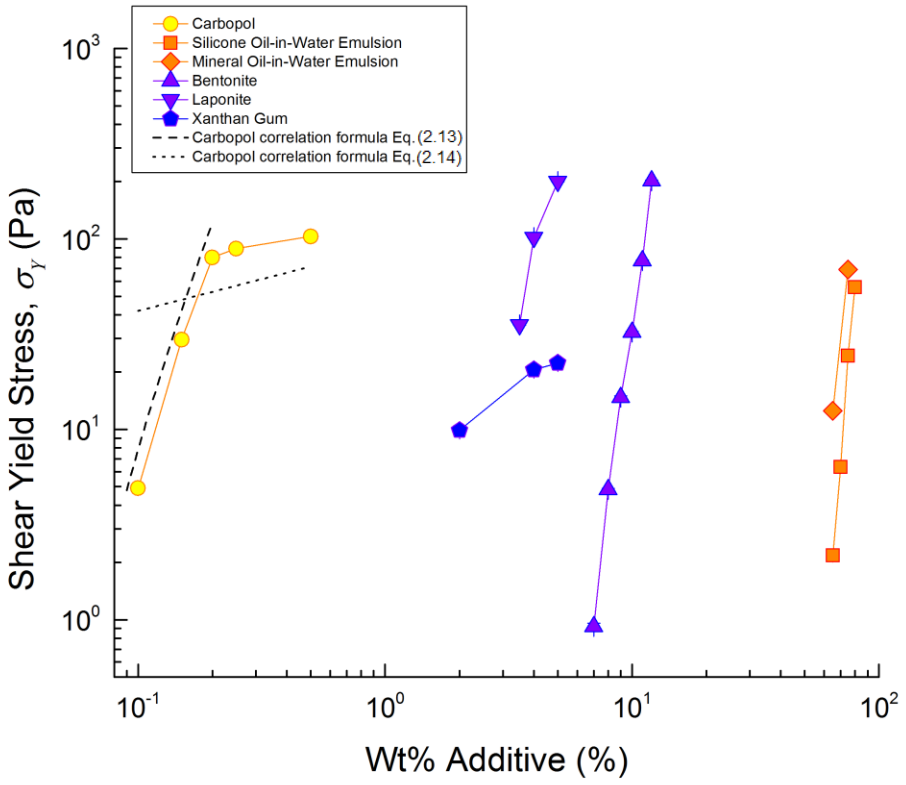

Figure 2.8. Shear Yield Stress versus wt% additive. Percentage of additive is not a parameter that represents the yield-stress behavior, however it is often crucial for achieving design targets. See Figure 2.5 and Appendix Figures for full steady shear flow data used for this plot.

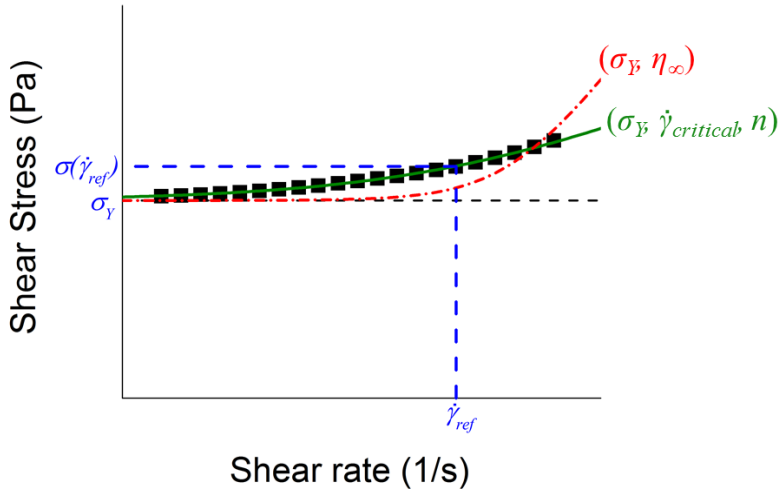

Figure 2.9. Low-dimensional representations of function-valued rheological data; here, a steady flow curve. Low-dimensional descriptions are required for easy comparison of materials when selecting or evaluating. More accurate representations can come at the cost of decreased physical meaning and added complexity. Here, three possible representations of a yield-stress fluid are shown: (blue dashed) two stress values, the yield stress and the stress at some reference shear-rate; (red dash-dot) the two-parameter Bingham model; and (green solid) the three-parameter Herschel-Bulkley model. (Data the same as in Figure 2.4.)

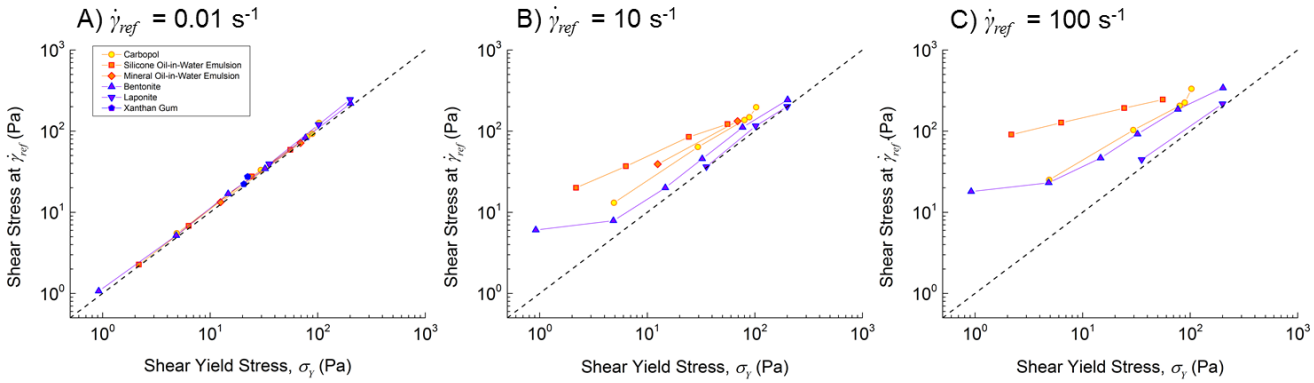

Figure 2.10. Ashby-style co-plot of low-dimensional yield-stress fluid descriptions: shear yield stress, σ_Y and steady shear stress at reference shear rates of 0.01, 10, and 100 s^{-1}.The dashed lines indicate flow stress equal to the yield stress. See Figure 2.5 and Appendix Figures for the full steady shear flow data.

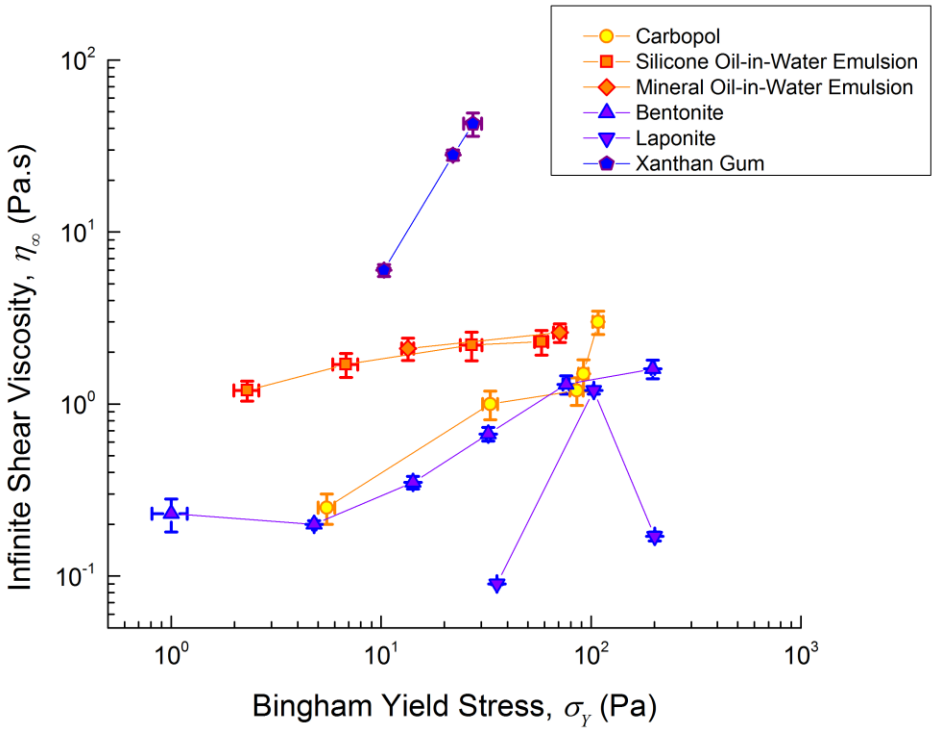

Figure 2.11. Ashby-style co-plots of the two-parameter Bingham model description of archetypal yield-stress fluids, $\sigma = \sigma_Y + \eta_\infty \dot{\gamma}$ (c.f. Figure 2.8, red dash-dot line). See Figure 2.5 and Appendix Figures for the full steady shear flow data which these Bingham parameters describe. Uncertainty bars indicate the standard error of the parameters from fitting.

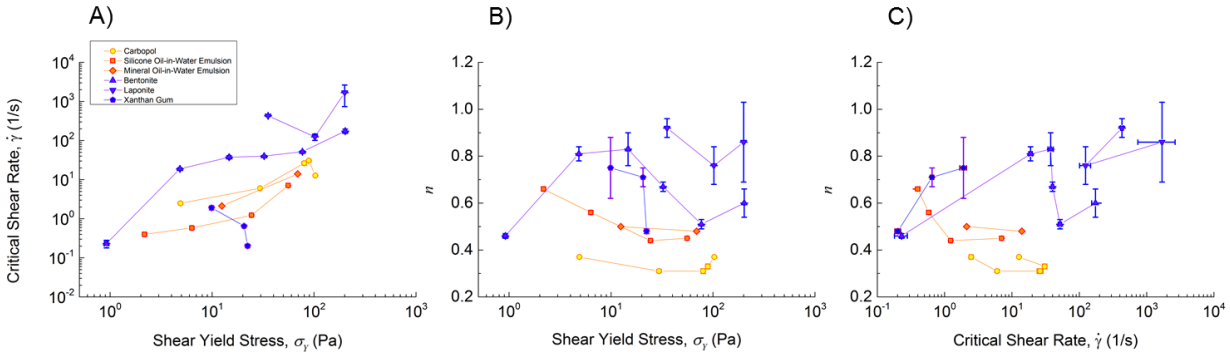

Figure 2.12. Ashby-style co-plots of an adaptation of the three-parameter Herschel-Bulkley model description of archetypal yield-stress fluids, $\sigma = \sigma_Y[1 + \left(\frac{\dot{\gamma}}{\dot{\gamma}_{critical}}\right)^n]$ (c.f. Figure 2.9, green solid line) where 'n' represents the degree of shear-thinning or shear-thickening. See Figure 2.5 and Appendix Figures for the full steady shear flow data which these Herschel-Bulkley parameters describe. Uncertainty bars indicate the standard error of the parameters from fitting.

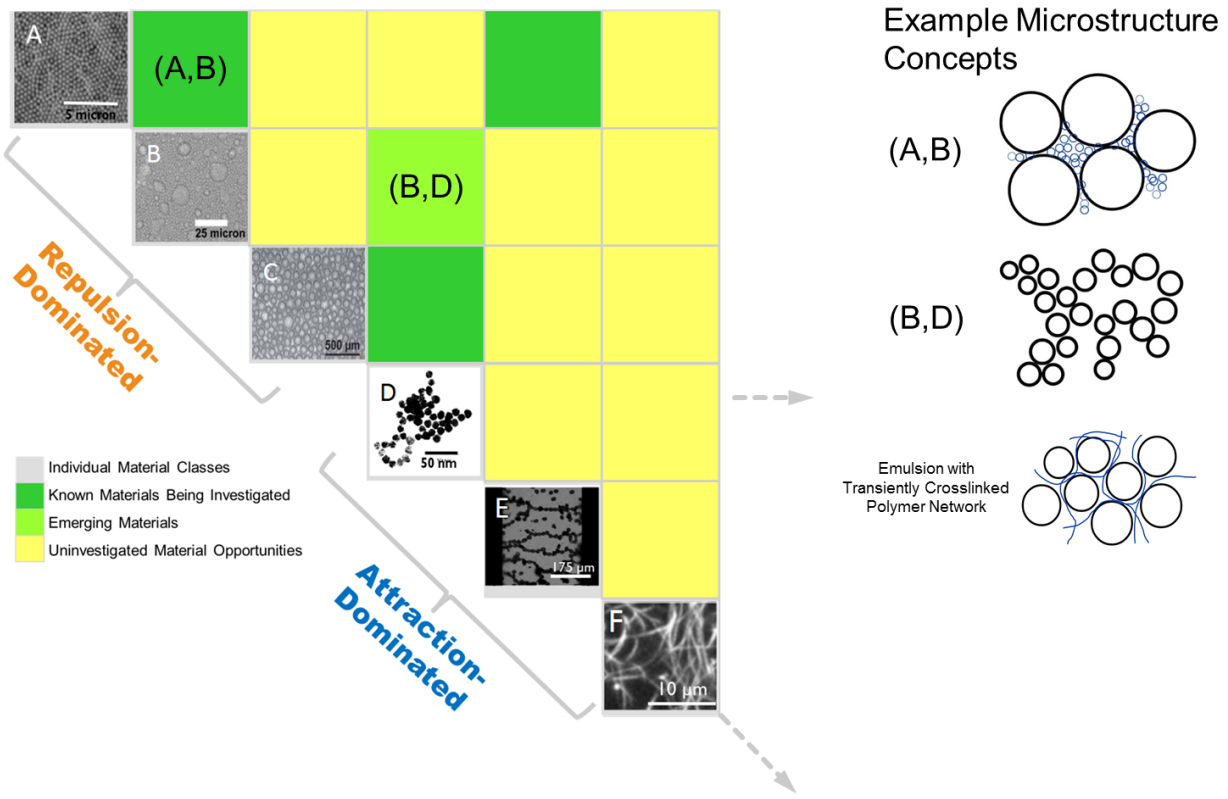

Figure 2.13. One possible concept generation strategy for material microstructures and combinations thereof. Each entry on the diagonal (same as Figure 2.7) represents an individual material class and serves as a label for off-diagonal combinations. Off-diagonal entries represent combinations of microstructures. Two example combinations are shown schematically: (A,B), a particulate suspension as the interstitial fluid in an emulsion; and (B,D), emulsified droplets networked in a structure similar to a particulate gel. A combination of an emulsion with a microstructure with no yield-stress, a transiently cross-linked polymer network, is shown on the right.

CHAPTER 3: Yield-Stress Fluids as Highly-Extensible Materials

3.1 Introduction

While oft-studied model yield-stress fluids can qualitatively reproduce the behavior of applications such as paint and condiments, the work here shows that many products and applications have behavior completely unlike any simply-formulated yield-stress model material. Materials like some chewing gums have a yield-stress but are also able to survive extremely large extensional deformations. Shown in Figure 3.1 is this obvious discrepancy between some of the most studied laboratory yield-stress fluid materials (Figure 3.1A) [26] and common industrial and consumer (application-relevant) yield-stress fluid materials (Figure 3.1B,C).

While previous studies of yield-stress fluids have been extensive, none have conceived of the materials as being highly-extensible. While there are certainly many yield-stress fluids that cannot survive large extensional strains, the works investigating yield-stress fluids in extension do not recognize materials that can [61,62]. This is an imbalance in the current paradigm of yield-stress fluids which we hope to rectify here by (i) introducing a method for characterizing the extensibility of yield-stress fluids, (ii) demonstrating the extent to which model materials differ from real materials in terms of extensibility, and (iii) introducing a simply-formulated material which is both highly-extensible and has a yield stress (Figure 3.1D).

3.2 Background

3.2.1 Extensional Rheology and Properties

The importance of characterizing the extensional properties of various materials has been recognized for biological fluids such as saliva [63], fluids used industrially in vibration dampers such as magnetic fluids [64], polymer processing with polymer solutions and melts [65], and consumer confectionary products such as chewing gum [66,67]. For the characterization of the extensional properties of these materials, the most common methods are the imposition of either a constant extensional strain rate or a step extensional strain (filament stretching or capillary breakup) [65,68]. Here we characterize materials by imposing a constant extensional strain rate in order to obtain the strain at which rupture occurs (strain-to-break). The two methods by which we impose extensional strain rates are by (i) exponentially increasing the separation velocity of two parallel plates (referred to here as "filament-stretching") and (ii) using a counter-rotating-drum fixture at a fixed velocity. For the filament-stretching experiments for initial radius, R_0 , and initial plate separation, L_0 , the aspect ratio,

$$\Lambda_0 = L_0 / R_0 , \tag{3.1}$$

should be approximately unity for homogeneous uniaxial extensional flow [69]. The counter-rotating-drum method was used when the filament-stretching experimental setup could not access the strain-to-break of a material (due to finite travel length). For length, L, true (Hencky) strain from,

$$d\varepsilon_{true} = \frac{dL}{L} \tag{3.2}$$

and engineering strain,

$$\varepsilon_{eng} = \frac{L_{final} - L_{initial}}{L_{initial}} \tag{3.3}$$

are related by,

$$\varepsilon_{true} = \ln(\varepsilon_{eng} + 1) \text{ [70].} \tag{3.4}$$

It must be noted that the metric by which we are determining the extensibility of these yield-stress fluids, the strain-to-break, is an *extrinsic* material property which will vary for different initial geometries. This is not to diminish the usefulness of this parameter as it is extremely useful in solid mechanics and material selection for comparing the ductility of materials through their "percent elongation" [71]. However, just as in the characterization of solid materials, care must be taken when comparing materials to standardize the initial sample geometry and extension rate, which we do here as much as possible.

3.2.2 Yield-Stress Fluids

For discussion on the controversy over the true existence of a yield stress, please refer to Section 2.2.3. For this paper, yield-stress characterization is performed in one of two ways depending on the sample: velocity-controlled steady flow tests, or step-stress creep compliance tests. Yield-stress parameters were obtained using the Herschel-Bulkley model described in Section 2.2.3. The organizational framework discussed in Section 2.4.1 is modified in Figure 3.2 to include combinations of microstructural mechanisms, the space that most application-relevant materials with complex formulations are likely to exist, though oftentimes their microstructure is simply unknown.

3.3 Materials and Methods

For preparation of the archetypal yield-stress fluids characterized and characterization using applied shear rate tests, please refer to Section 2.3.

For our proposed model material, hereafter referred to as a PVA-borax emulsion, the same 1000 cSt silicone oil used previously was blended using an overhead stirrer at 300 rpm for 5 minutes with a 4%wt solution of poly(vinyl alcohol) (molecular weight 85,000 – 124,000, 99+% hydrolyzed) in water and then added to a test tube containing a 4%wt solution of sodium tetraborate in water and shaken vigorously and occasionally stirred for 5 minutes. The poly(vinyl alcohol) and sodium tetraborate were both purchased from Sigma-Aldrich. The application-relevant materials tested were Nutella; whipped cake frosting from Duncan Hines; Laffy Taffy; HubbaBubba Tape; and HexArmor resin, a material used in the production of personal protective equipment. All application-relevant materials were tested as received. The Laffy Taffy and HubbaBubba Tape were tested in shear and extension at 37 °C, an average person's mouth temperature.

As shown in Figure 3.3, for materials prone to edge failure at high shear-rates, a series of step-stress creep tests were imposed. Materials were allowed to reach a steady shear-rate allowing for the determination of the steady shear viscosity as a function of the applied stress. The yield stress in this case was taken from within the stress range over which the viscosity begins to steeply decline. Note that since no simple correction is available for step-stress tests with parallel disks, the yield stresses of the two materials tested in creep are apparent stresses rather than true stresses.

Characterization with filament-stretching for the extensional strain-to-break was performed on a TA Instruments ARES-G2 rotational rheometer (separated rotational

motor/transducer, combined axial motor/transducer). For the filament-stretching experiments a parallel-plate geometry with a diameter of 8 millimeters and advanced peltier system bottom plate were used. The samples were loaded at a gap of 4 millimeters resulting in an aspect ratio, $\Lambda_0 = 1$. The maximum gap on the ARES-G2 allowed for a maximum engineering strain of $\varepsilon_{eng} = 2000\%$. A constant Hencky strain rate, $\dot{\varepsilon} = 0.2s^{-1}$, was used for all tests.

The counter-rotating-drum experiments were performed on the previously mentioned DHR-3 using an SER2 Universal Testing Platform fixture from Xpansion Instruments. For the counter-rotating-drum experiments, samples were loaded as per the recommended dimensions and procedure [72]. A constant Hencky strain rate, $\dot{\varepsilon} = 0.2s^{-1}$, was used for all tests.

Videos were taken during all extensional tests. Images were correlated with the measured load and displacement in order to determine the extensional strain-to-break.

3.4 Results

3.4.1 Archetypal Yield-Stress Fluids and Application-Relevant Materials

The shear and extensional behavior of the studied archetypal yield-stress fluids are shown in Figure 3.4 with images of representative systems just before rupture occurs. All data points in Figure 3.4 are simplified descriptions of the full data from shear flow (Figure 3.5, Appendix Figures 1-6) and extensional flow (Figure 3.6, Appendix Figures 7-12). The steady simple shear flow characterization for the three representative systems in Figure 3.4 is shown in Figure 3.5, while the extensibility characterization is shown in Figure 3.6. While these materials span a range of yield stresses of over two decades, the engineering strain-to-break varies by approximately a factor of two.

In Figure 3.4, there is no clear correlation between the extensibility and yield-stress for the data set taken as a whole, yet correlations can be seen within distinct material systems. Carbopol and the silicone oil-in-water emulsions, both repulsion-dominated systems, show a slight increase in extensibility as their yield stress increases, with the extensibility of Carbopol saturating at the same time its yield stress saturates. The extensibility of Bentonite and the mineral oil-in-water emulsions are essentially flat as their yield stress is increased. Laponite is the one tested system that shows a decrease in extensibility as the yield stress is increased. Xanthan gum as a long-chain polymer system shows the largest extensibility, as may be expected from a stretchy attractive network. However, as Figure 3.4B shows, even the extensibility of Xanthan gum is nowhere near the extensibility behavior seen for the application-relevant materials in Figures 3.1B and 3.1C (though Xanthan does show somewhat similar necking behavior to Figure 3.1B).

Qualitatively, Figure 3.1A (Bentonite), the system with the lowest yield-stress of those pictured, looks very similar to water and in this regard compares well to the pictured water break-up limit under zero gravity of 138% [73]. For the values taken from simulations for the 3D tensorial Herschel-Bulkley model [61], the surface tension of water was used as all of our material systems have a continuous water-phase. For those simulations, an aspect ratio of $\Lambda_0 = 2$ was used and thus a smaller strain-to-break is expected. The simulations show non-monotonic behavior, with ε_{break} varying by at most a factor of two, similar to many of the archetypal materials.

As shown in Figure 3.1, when considering application-relevant materials, the strain limit for the filament-stretching experimental method was reached for some materials and thus it was

necessary to make use of the counter-rotating-drum experimental setup shown in Figure 3.7. Comparing the consumer products to the archetypal fluids in Figure 3.8, it can be seen that while the laboratory systems approach the behaviors of Nutella and whipped frosting, they come nowhere near the HexArmor resin or confectionary products. Thus, archetypal model materials and mathematical constitutive models may be irrelevant for application-relevant understanding in which physics associated with high extensibility is required.

3.4.2 Design and Analysis of a Model Material

In attempting to match the performance of the materials like those shown in Figure 3.1B and 3.1C with a material with an easily controllable formulation, we made use of the methodology outlined in Section 2. The design methodology presented contrasts with analysis strategies in that it is built upon generic principles of inverse problem solving: the performance objective (material behavior) is specified in a chemistry- and structure-agnostic way, allowing for creative concept generation. Ideally, in the design process one would be able to easily select materials which matched the necessary properties from a material database, however, since the paradigm of yield-stress fluids as highly-extensible materials has been so under-developed, we had to carry out the analysis/characterization (described in previous sub-section) ourselves. As we have shown, none of the surveyed archetypal yield-stress fluids were capable of achieving the properties or performance displayed by the application-relevant materials, thus our only choice was to formulate a new material. For this process numerous microstructure concepts were envisioned using a technique of juxtaposing two different existing microstructures. The material concept we chose to develop is shown in Figure 3.9 and was conceived of as the combination of a yield-stress-providing microstructure (a packed emulsion), and an extensibility-providing microstructure (a transiently-cross-linked network). The actual microstructure of the PVA-borax

emulsions we have synthesized have yet to be characterized, however based on this concept we were able to achieve the performance shown in Figure 9 which is able to match the extensibility of existing application-relevant materials.

Figures 3.10 and 3.11 show the steady simple shear flow characterization for the PVA-borax emulsions with three different oil loadings. The material transitions above 50%wt oil from a shear-thinning material with no yield stress to a yield-stress fluid with yield stresses of 103 Pa, and 310 Pa shown for the 55 and 60%wt oil formulations, respectively. Though these materials are able to achieve the yield stress performance objectives we sought, there are numerous experimental challenges with the system which are shown in Figure 3.11. In shear, the two formulations showed two different experimental artifacts. In Figure 3.11A, the 55%wt oil system shows a higher measured stress at a smaller gap indicating a confinement effect, while in Figure 3.11B, the 60%wt oil system showed a lower measured stress at a smaller gap indicating a slip effect. Additionally, similarly to the image of gum shown in Figure 3.6, both formulations show edge fracture at higher shear rates, limiting the available experimental window.

Figure 3.12 shows the characterization of the PVA-borax emulsions in extension in both the filament-stretching and counter-rotating-drum experimental setups. As was desired for matching the behavior of the application-relevant products, the 55wt% oil reached the strain-limit of the filament-stretching setup and thus necessitated testing on the counter-rotating-drums. Due to the softness of the material, reproducible loading was extremely challenging for both formulations, resulting in the large error bars shown. The characterization results for the designed yield-stress fluid system are shown compared to archetypal and consumer/industrial yield-stress fluids in Figure 3.13. With our synthesized material we were able to match the extensibility performance of the most extensible application-relevant material shown here.

3.5 Conclusions

Here we have presented a new paradigm of yield-stress fluids as capable of being highly-extensible materials. We introduced a methodology for characterizing yield-stress fluids capable of capturing a wide range of yield stress and extensibility behavior. Based on our characterization results, it can be seen that yield-stress fluids commonly studied in laboratory settings are not capable of representing the behavior of many industrial and consumer products. Lacking a suitable model for these products which have complex formulations, we generated a concept for a new material based on the combination of microstructures, synthesized our candidate material, and then carried out rheological characterization. Though there are numerous experimental challenges associated with the newly synthesized material, we have shown that it is capable of quantitatively matching the behavior of highly-extensible yield-stress fluid application-relevant materials. Schematic relations of the design and analysis processes we carried out are shown in Figure 3.14.

When studying applications where extensibility is important, we have shown here that the archetypal yield-stress fluids are not acceptable models and have provided a candidate model material for study. However, we have also shown that the inverse is true, when studying applications where extensibility is neglected, one has the choice of many well-characterized model materials and need not worry about the physics associated with high extensibility. For the high-extensibility materials, new constitutive models are required that do capture the appropriate physics.

Shown here are only a few material formulations, and thus the full performance space available for our designed system is unknown and is certainly un-optimized, not to mention the

plethora of un-synthesized or even un-considered materials which may also match the target performance. As stated when introducing our characterization method, the results are dependent on initial geometry and extension rate. Though our initial geometry was chosen in order to have a near-optimal initial aspect ratio, our choice of extension rate was somewhat arbitrary. It has yet to be investigated what effect extension rate has on the extensibility of yield-stress fluids.

3.6 Figures and Tables

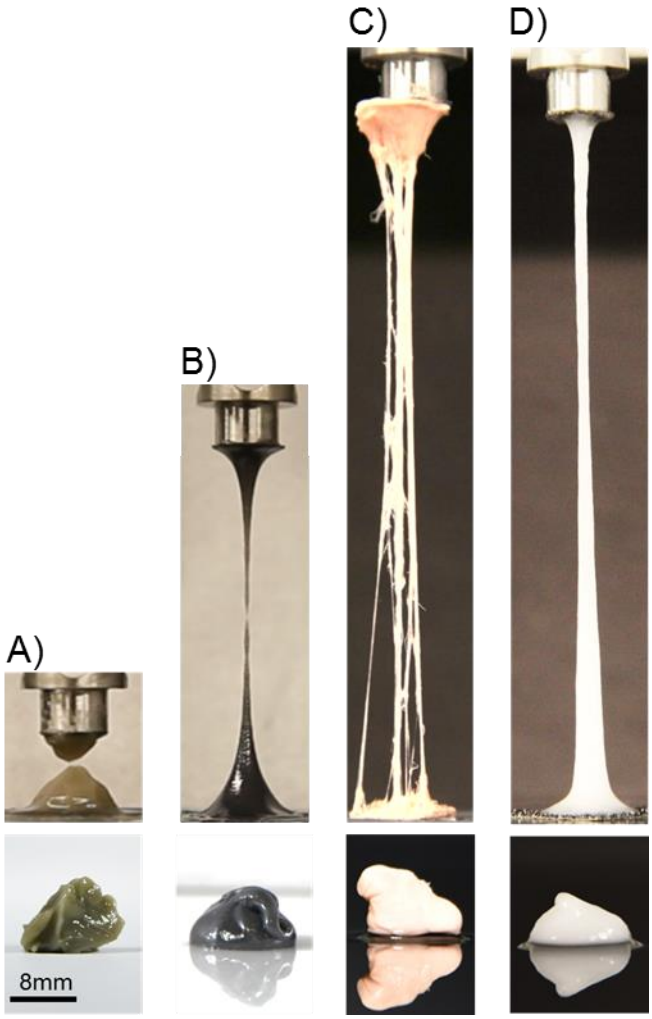

Figure 3.1. The extensional and resting behavior of various yield-stress fluids are shown. Shown in column A) is Bentonite, a material commonly studied as a model yield-stress fluid in laboratory settings. Columns B) and C) show yield-stress fluids used in application-relevant products, a resin used in printing by the company HexArmor; and the bubble gum, HubbaBubba Tape, respectively. The bottom row of pictures all suggest the nature of these materials as yield-stress fluids since contours and corners are held for timescales longer than tens of minutes and in this respect the materials only differ moderately in their observed behavior. The top row of pictures show the behavior of these materials in extension. Shown in A) and B) are the materials immediately after rupture occurs. The materials shown in C) and D) both resisted rupture to the limit of the experimental setup. Due to the clear difference in extensional behavior of the common yield-stress fluids and the standard model yield-stress fluid, here we suggest the material shown in Column D), a silicone oil-in-water emulsion with a transiently-cross-linked network of poly(vinyl alcohol), as a model for studying the behavior of highly-extensible yield-stress fluids. The scale bar shown applies to all images.

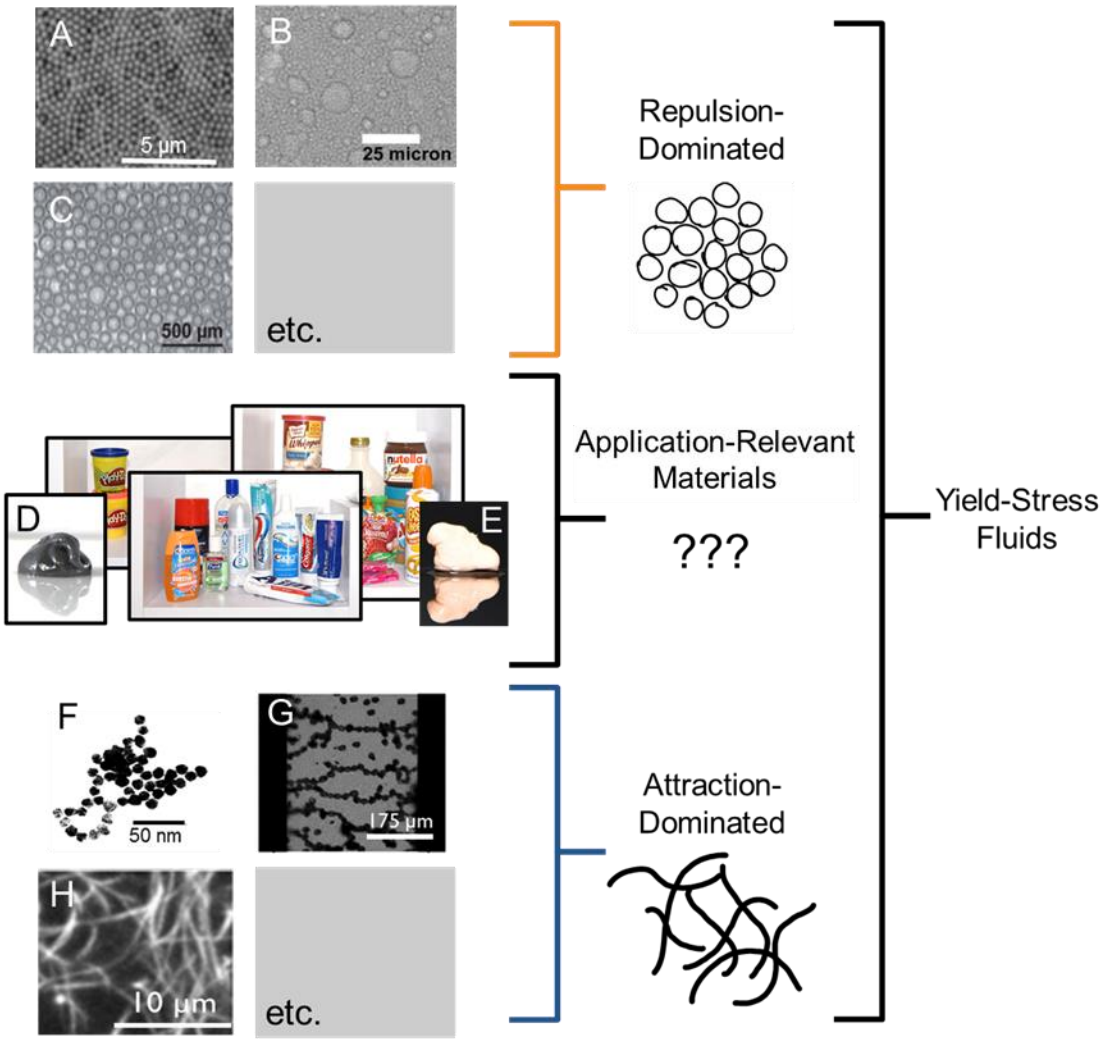

Figure 3.2. Design strategies for yield-stress fluid design organized into 'repulsion-dominated' and 'attraction-dominated' (although combinations also exist). For most application-relevant materials the microstructural mechanism governing the yield stress is unknown. The materials pictured include toothpaste, shaving cream, playdoh, spray cheese, and apple sauce, all of which are yield-stress fluids. Images shown are (A) particulate suspensions [49], (B) emulsions [42], (C) foams [50], (D) HexArmor resin, (E) HubbaBubba Tape, (F) particulate gels [48], (G) electro/magneto-rheological fluids [51], and (H) fiber gels [53].

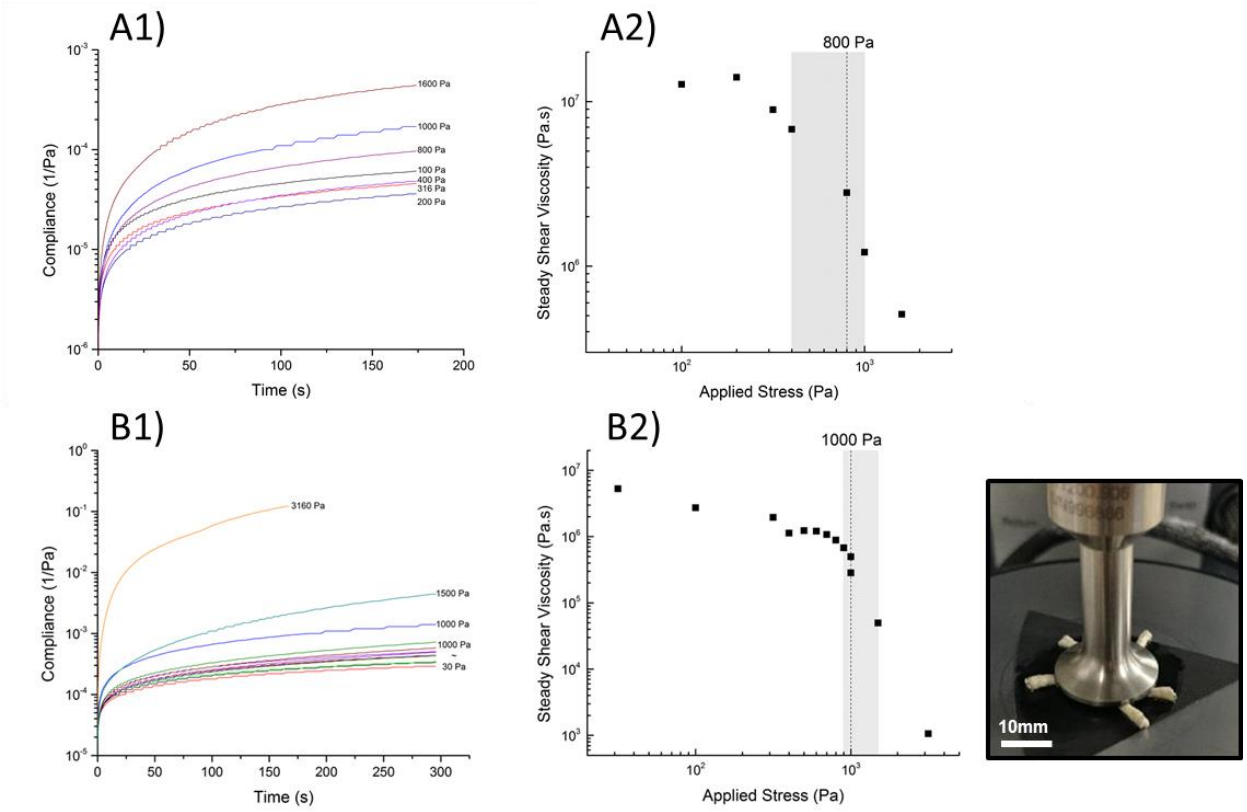

Figure 3.3. Shear creep compliance curves for difficult-to-test materials, A) Laffy Taffy, and B) HubbaBubba Tape. Velocity-controlled flow tests were not feasible for these materials due to edge failure behavior as pictured on the right for gum. Because of this, constant applied stress tests were used to obtain the compliance over time (A1 and B1), resulting in steady shear viscosity curves (A2 and B2) which show gradual yielding. The grey shaded regions are bounded by the stresses over which viscosity has begun to decrease substantially, the yield stress for each material is taken as the stress for the data point within the shaded regions.

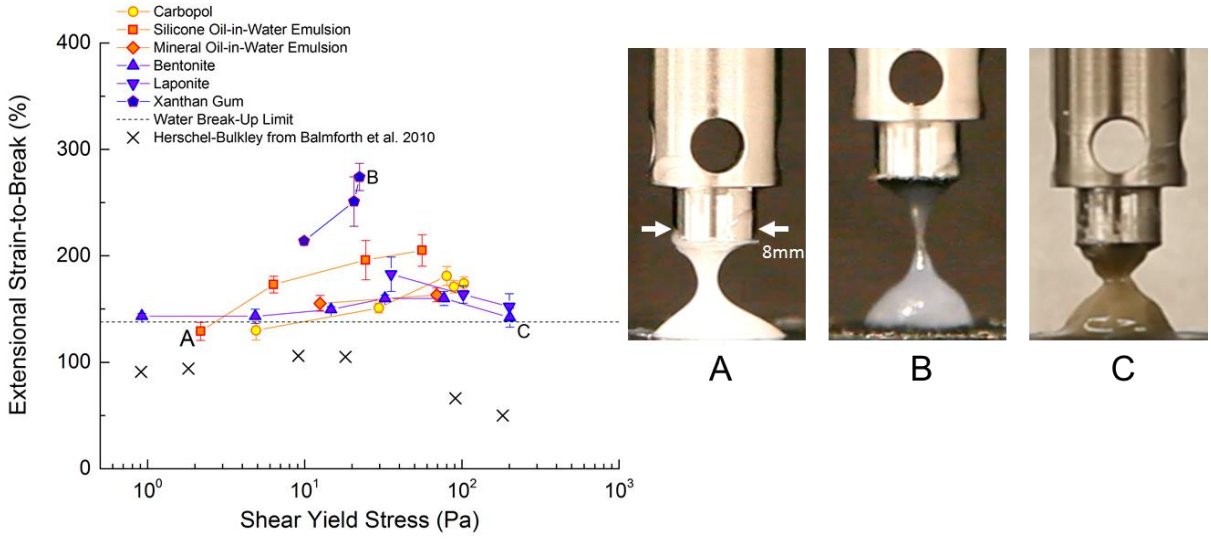

Figure 3.4. Ashby-style co-plot of the shear and extensional behavior of archetypal yield-stress fluids. See Appendix Figures for the full steady flow data with Herschel-Bulkley model fit to determine the shear-yield-stress parameter. Transient extensional tests (see Appendix Figures for stress response) were correlated with images to obtain the extensional strain-to-break parameter. Shown are three representative materials: A) a silicone oil-in-water emulsion that is 65wt% oil, B) 5%wt xanthan gum in water, and C) 12wt% bentonite in water. Error bars are the result of repeated experiments. The water break-up limit for a volume equivalent to those in our experiments is 138% and was determined for zero-gravity conditions [73]. The values from [61] were found using a Herschel-Bulkley model for an initial aspect ratio double that of our experiments.

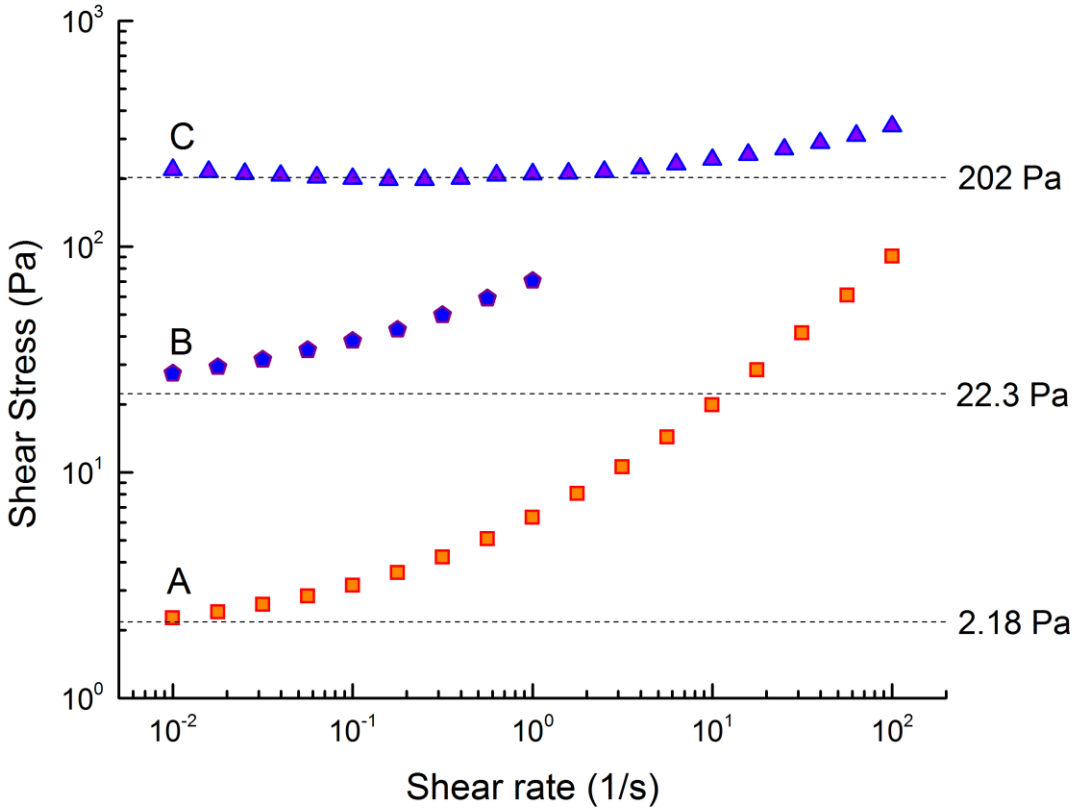

Figure 3.5. Steady simple shear flow for the three materials shown in Figure 3.4. Lines between data points are a guide to the eye. A velocity-controlled test from high-to-low shear rates was used for materials A and C. A low-to-high shear rate was used for material B. The dashed lines show the fit yield-stress parameter for each material.

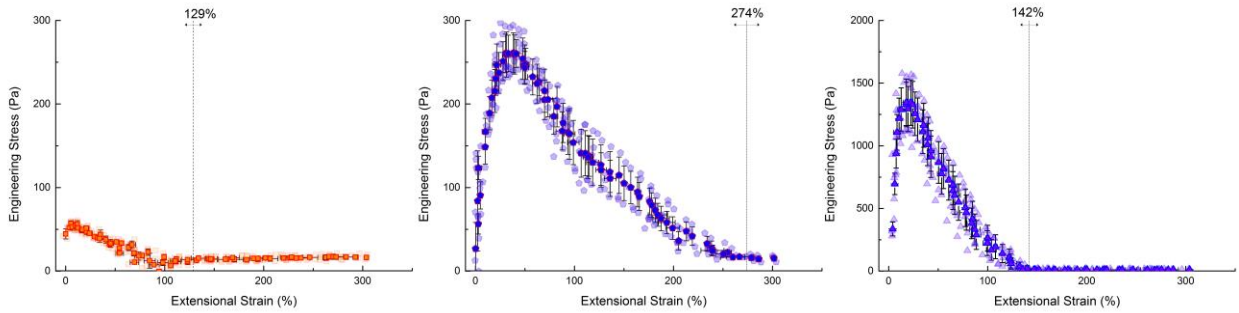

Figure 3.6. Extensional engineering stress curves for the three materials shown in Figure 3.4 tested using the ARES-G2 filament stretching experimental setup. The bold data points are the average of repeated experiments (faded data points) which provide the error bars. The vertical dashed lines depict the average strain-to-break which was found by correlating the extensional stress curves with video images. The horizontal arrows below the strain-to-break labels depict the standard deviation in the strain-to-break from repeated experiments. A constant Hencky strain-rate of $\dot{\varepsilon} = 0.2$ was used for all extensional tests.

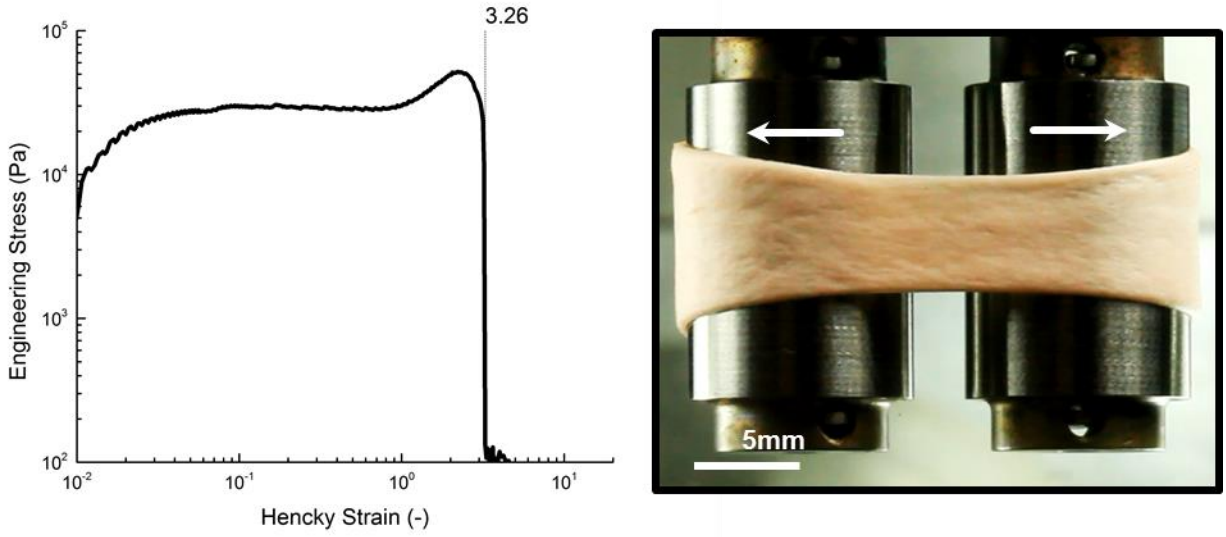

Figure 3.7. Extensional engineering stress versus Hencky strain for a commercial product, HubbaBubba Tape. Extensional data for materials which reach the limit of extensibility for the ARES-G2 filament stretching experimental setup (shown in Figure 3.1) were obtained using an SER2 counter-rotating-drum stretching experiment as shown on the right. The dashed line indicates the strain-to-break. For comparison with other materials, the Hencky strain was related to engineering strain with Equation (4).

Table 3.1. All presented material formulations organized by material and weight-percentage of additive. For specific synthesis procedure refer to Sections 2.3 and 3.3.

Material	Formulation
Carbopol	Specified weight-percentage of Carbopol 940 in distilled water, neutralized to pH 7 with sodium hydroxide
0.1%wt	
0.15%wt	
0.2%wt	
0.25%wt	
0.5%wt	
Silicone Oil-in-Water Emulsion	
65%wt	65wt% silicone oil, 23.33wt% deionized water, 11.67% sodium dodecyl sulfate
70%wt	70wt% silicone oil, 20wt% deionized water, 10wt% sodium dodecyl sulfate
75%wt	75wt% silicone oil, 16.67wt% deionized water, 8.33wt% sodium dodecyl sulfate
80%wt	80wt% silicone oil, 13.33wt% deionized water, 6.67wt% sodium dodecyl sulfate
Mineral Oil-in-Water Emulsion	
65%wt	65wt% mineral oil, 23.33wt% deionized water, 11.67% sodium dodecyl sulfate
75%wt	75wt% silicone oil, 16.67wt% deionized water, 8.33wt% sodium dodecyl sulfate
Bentonite	Specified weight-percentage of Bentonite in distilled water
7%wt	
8%wt	
9%wt	
10%wt	
11%wt	
12%wt	
Laponite	Specified weight-percentage of Laponite RD in distilled water
3.5%wt	
4%wt	
5%wt	
Xanthan Gum	Specified weight-percentage of xanthan gum from *Xanthomonas Campestris* in deionized water
2%wt	
4%wt	
5%wt	
PVA-Borax Emulsion	
50%wt	50wt% silicone oil, 1wt% poly(vinyl alcohol), 1wt% borax, 48wt% deionized water
55%wt	55wt% silicone oil, 0.9wt% poly(vinyl alcohol), 0.9wt% borax, 47.8wt% deionized water
60%wt	60wt% silicone oil, 0.8wt% poly(vinyl alcohol), 0.8wt% borax, 47.6wt% deionized water

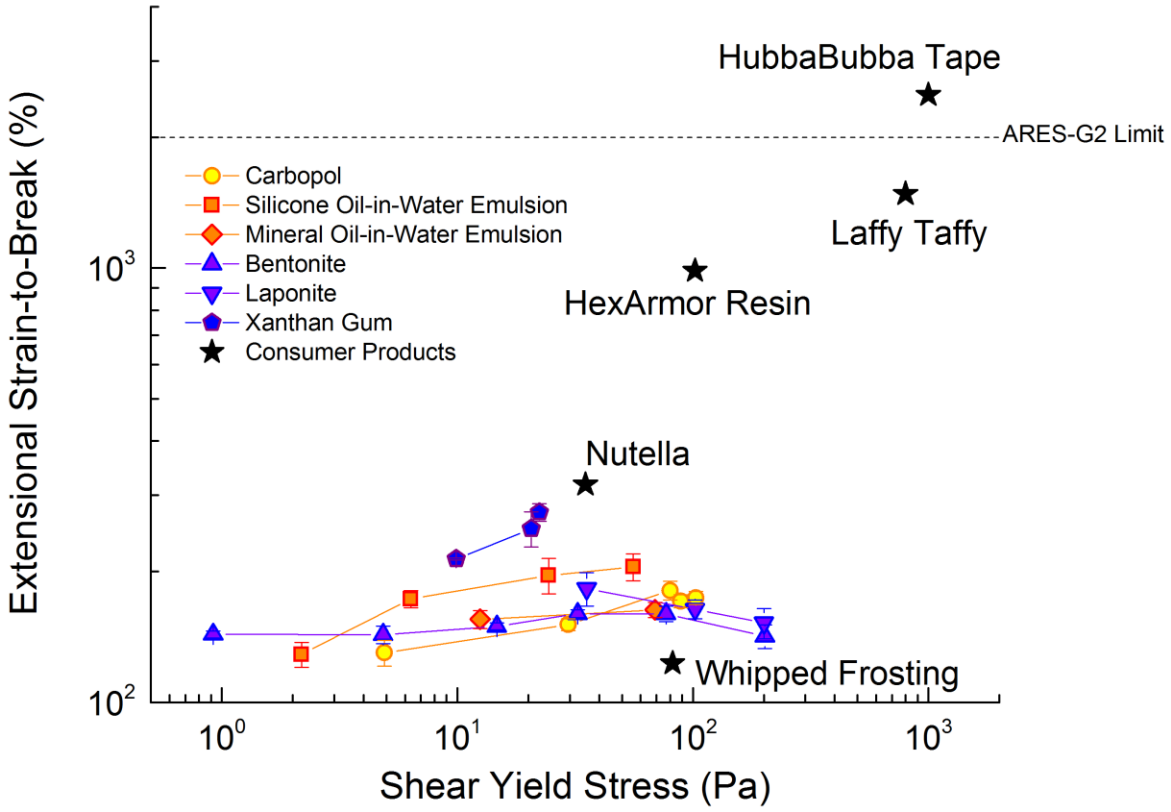

Figure 3.8. Ashby-style co-plot of archetypal yield-stress fluids and consumer products. See Appendix Figures for the full steady flow and extensional engineering stress curves that these points represent. Repeated experiments were not performed for consumer products which thus lack error bars. Note that, compared to Figure 3.4, both axes are log scale.

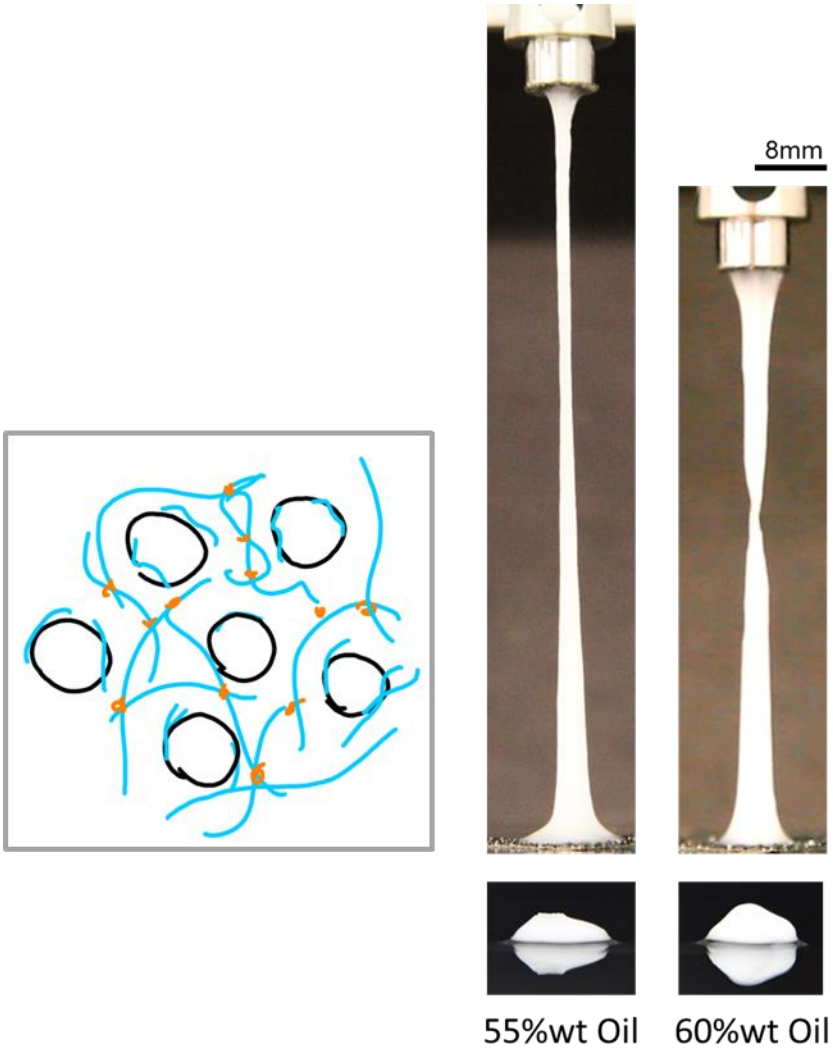

Figure 3.9. Proposed model highly-extensible yield-stress fluid, a silicone oil-in-water emulsion combined with a transiently-cross-linked network of polyvinyl alcohol. Shown on the left is a sketch of the microstructural concept used to conceive of this material: the emulsified droplets (shown in black) provide the material with a structure with which to bear static loads (a yield stress), while the transiently-cross-linked polymer network (blue lines with orange crosslinks) prevents the droplets from coalescing and allows the structure to survive large extensional strains. Shown on the right are the two synthesized formulations which manifested the desired qualitative performance objectives. The 8mm scale bar shown applies to all four images on the right.

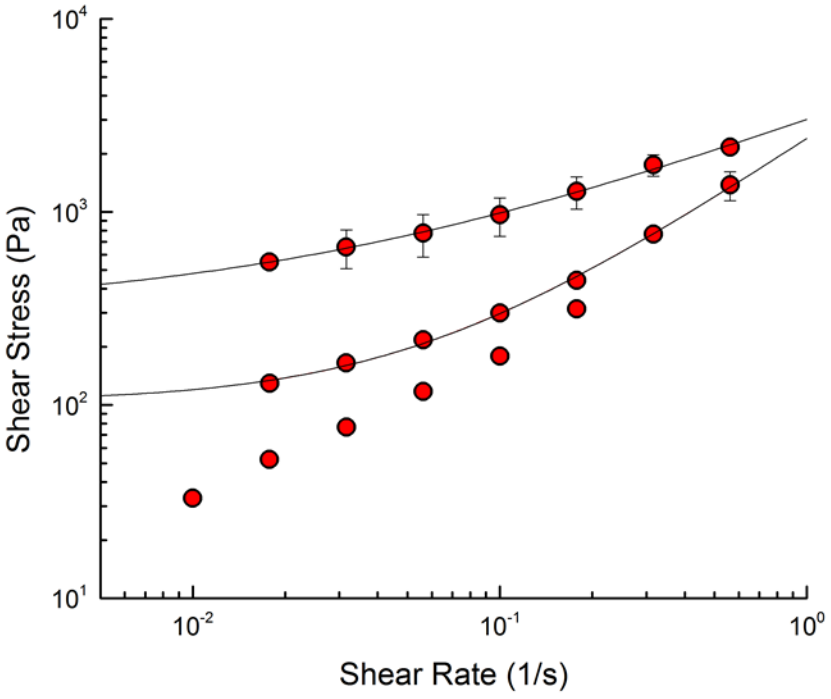

Figure 3.10. Steady simple shear flow from low to high shear rate at a gap of 500μm for three formulations of the proposed model material made with 50, 55, and 60%wt Silicone Oil. Increasing the oil droplet concentration results in increased flow stress. Lines indicate the fit to a Herschel-Bulkley model. Error bars are the result of repeated experiments. The 50%wt oil concentration did not show a yield stress and was not repeatedly tested.

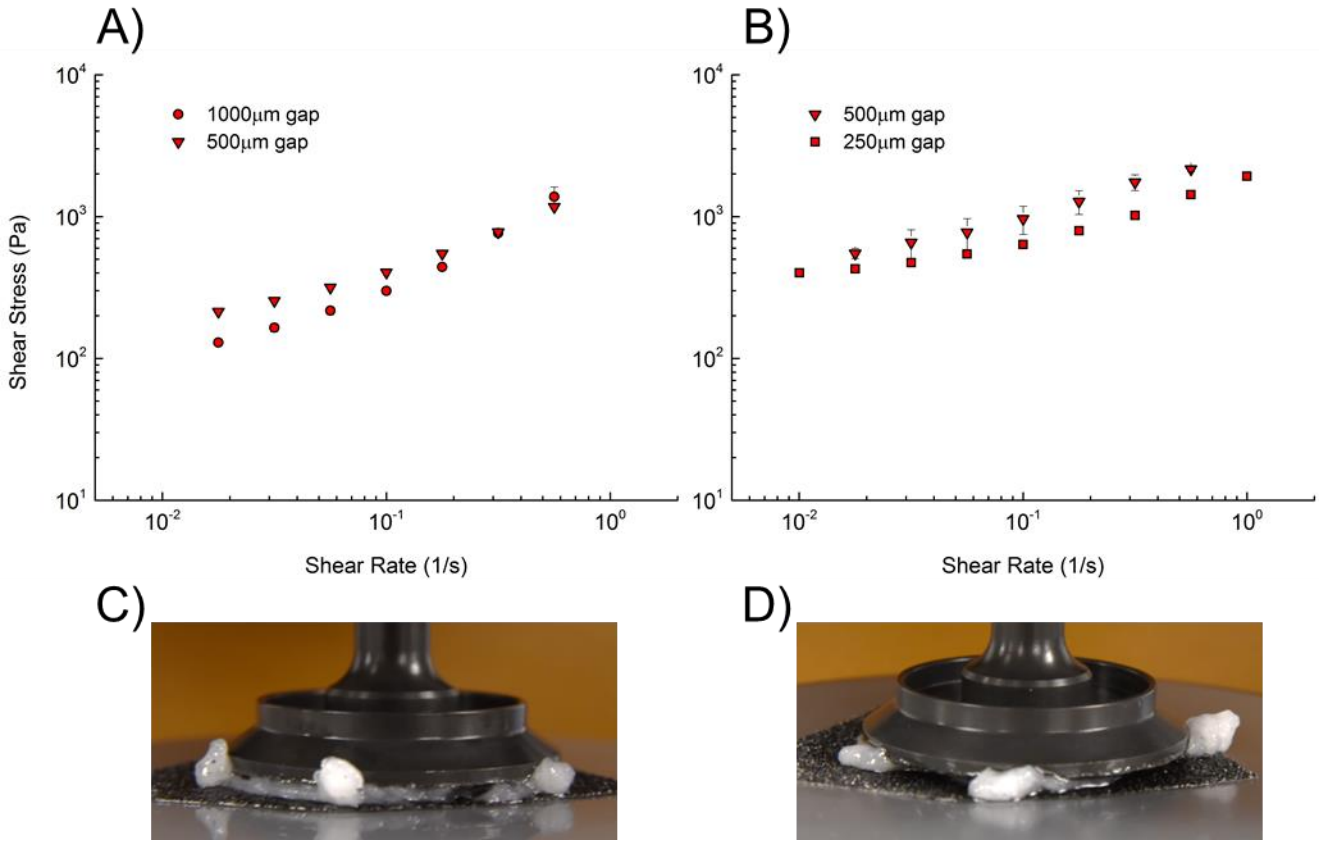

Figure 3.11. Experimental challenges with the proposed model elastic yield-stress fluid system. Shown in A) for the 55%wt oil system and in B) for the 60%wt oil system are observed experimental artifacts. A) Shows a confinement effect (lower gap shows higher flow *stress*), while B) shows a slip effect (lower gap shows higher apparent *shear rate*). C) and D) show sample fracture at shear rates higher than 1 s^{-1} limiting the available observable ranges for the 55 and 60%wt oil system respectively. Data points when edge failure was observed are not reported. The diameter of the plate in C and D is 40mm.

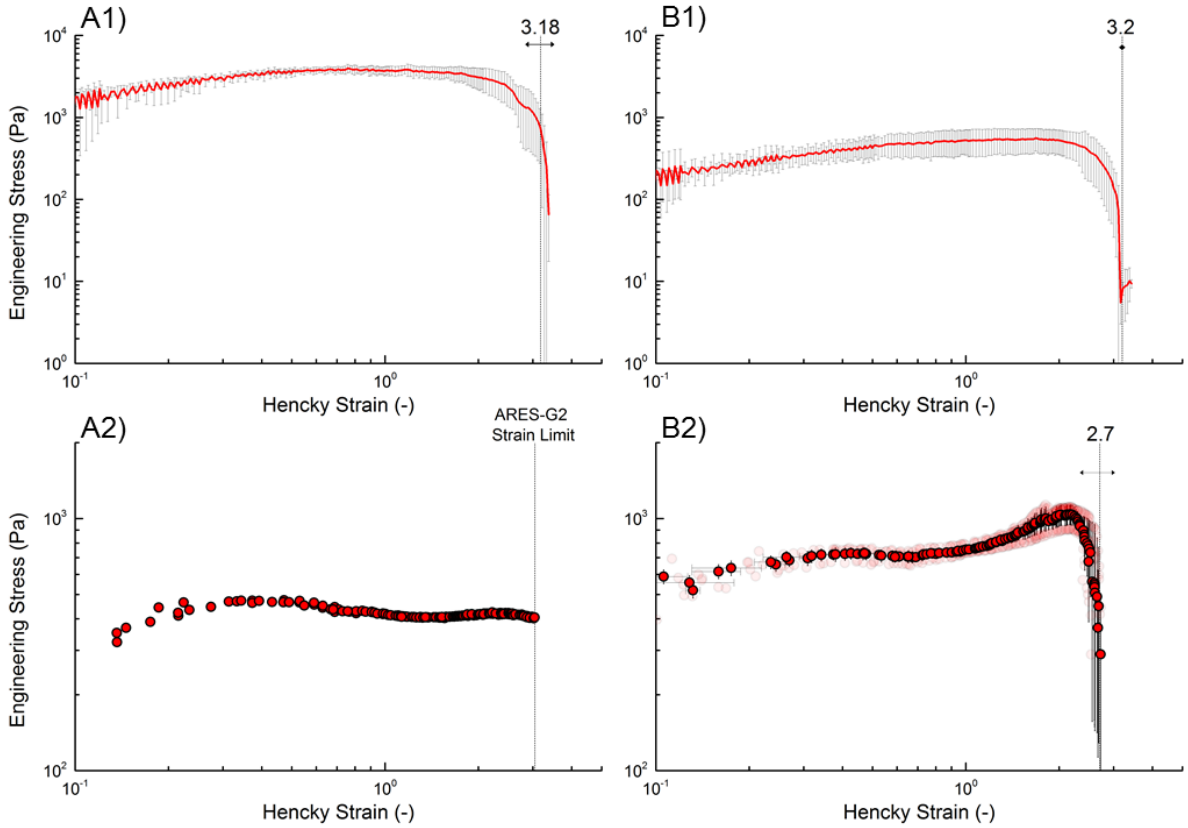

Figure 3.12. Extensional engineering stress curves for proposed model highly-extensible yield-stress fluid. A) 55%wt and B) 60%wt formulation. A1) and B1) depict experiments performed using the SER2 experimental setup with the average of repeated experiments in red and error bars in gray. A2) and B2) depict experiments performed using the ARES-G2 experimental setup with bold data points showing the average of repeated experiments (faded data points) which provide the error bars. Curves were correlated with video in order to determine the engineering strain-to-break. Error bars shown are from repeated experiments. Since the 55%wt Oil formulation reached the ARES-G2 strain limit (bottom-left corner), repeat measurements were not performed with that experimental setup.

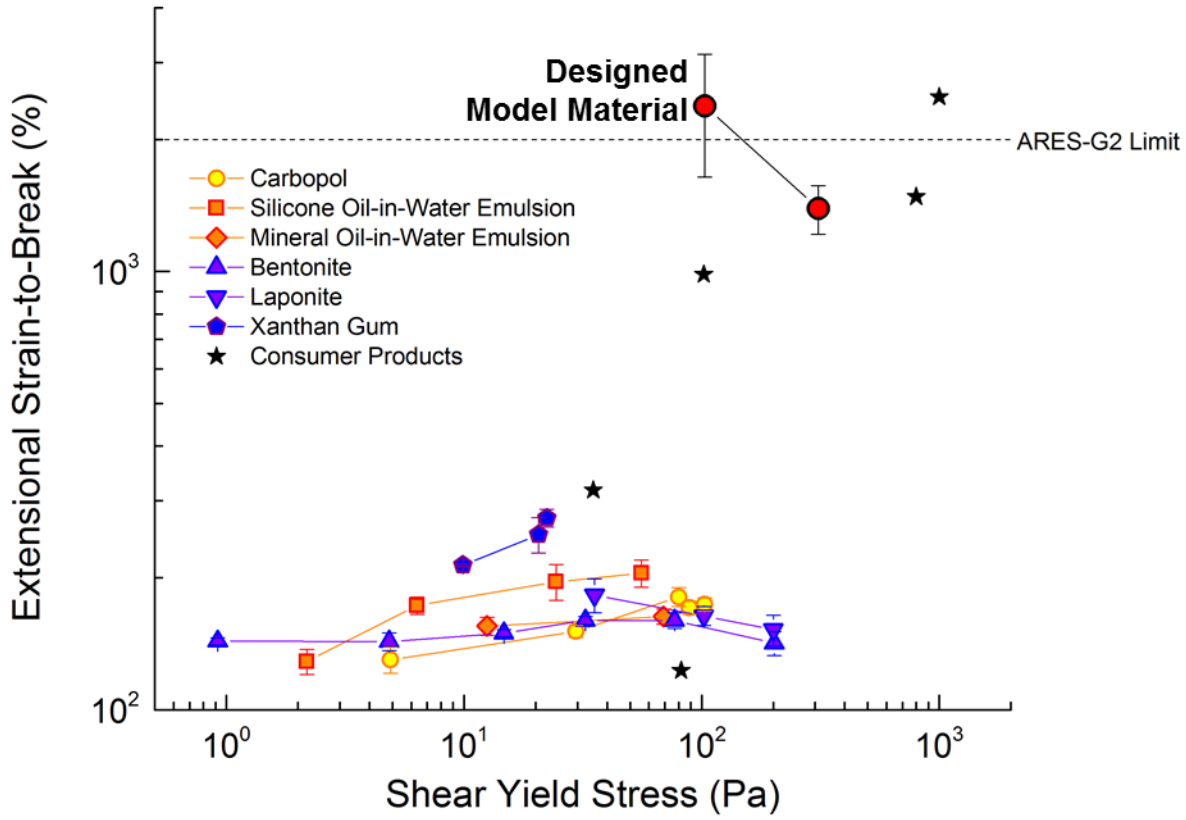

Figure 3.13. Ashby-style co-plot of all materials studied here. See Appendix Figures for the full steady flow and extensional engineering stress curves that these points represent. For the most direct comparison, the strain-to-break value used was taken from the ARES-G2 experimental setup whenever possible.

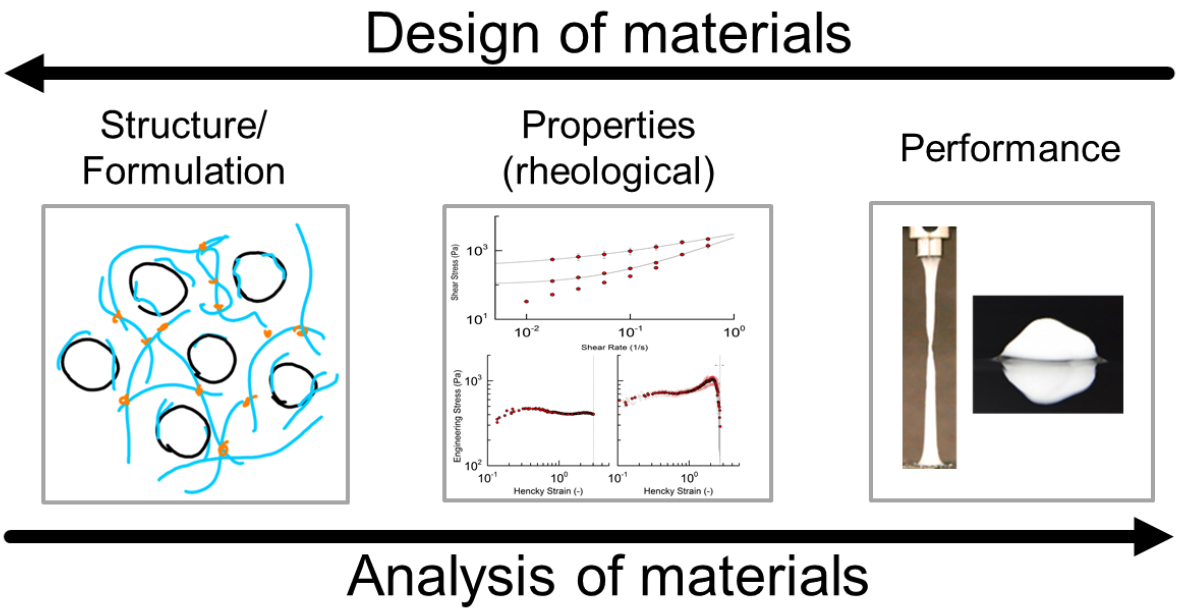

Figure 3.14. Schematic relations of design and analysis of materials (adapted from [7] and applied to rheological properties). Analysis starts on the left with a specific material structure and connects it to properties and performance which is non-trivial for rheologically-complex materials. Design starts with a desired performance, and a decision is made on what properties are desired and what material to best achieve it. The process presented in this work demonstrates the complementary nature of analysis and design. Starting with the observable performance goal (on the right) of yield-stress fluids that are highly extensible (Figure 3.1B,C), attempts were made to match this by analyzing and evaluating simple model systems (Figure 3.2); when this failed a new microstructure concept was conceived and formulated (on left, also Figure 3.9), and then that too was analyzed for validation that the performance goal had been met. Following these principles we have demonstrated the design process of a new material that is built upon a strong foundation of analysis.

CHAPTER 4: Conclusions and Future Work

Here, two new paradigms of yield-stress fluids have been presented: one that is useful from a design perspective, and one of yield-stress fluids as capable of being highly-extensible. By applying generic design principles, a formulation- and structure- agnostic functional objective was introduced which gives rise to an organization based on the structural mechanisms of yield-stress fluids (Figure 2.7), and methodologies for concept generation and evaluation were presented (Figures 2.8, 2.10, 2.11, 2.12, 2.13). Following this design methodology and introducing a characterization method for the extensibility of yield-stress fluids, it was found that no common model materials are highly-extensible, and that the current paradigm of yield-stress fluids extensibility is incapable of capturing the high-extensibility seen in many application-relevant materials (Figure 3.1). Thus, a new material concept capable of high-extensibility was generated, formulated, and characterized (Figure 3.9). Whether designing or analyzing yield-stress fluids it must be considered whether extensibility should be included and appropriate model materials or constitutive equations chosen or developed.

The design methodology introduced here, while applied towards a highly-extensible yield-stress fluid, is generic enough to be applied to any other secondary property of yield-stress fluids, or even other rheologically complex phenomena. The presented design database and material property scaling laws (Table 2.2) are useful though incomplete tools for designing yield-stress fluids, but when attempting to design with any rheologically complex material one should follow the general principle of considering all possible concepts and only selecting a concept that is justifiably superior to other options.

The material formulation introduced here was not optimized and the full formulation space was unexplored. In the future, the design of complex materials will involve at least two optimization stages: based on the structure- and material-agnostic design specifications an optimal rheology or rheologies must be determined, and then the chosen concept formulation and structure must be optimized. All of the design work must of course still be complemented by the relevant analysis/characterization of the proposed material for iterative or validation purposes. The characterization method we introduced here obtains a metric that is relevant to the extensibility of a material, but for more complicated design objectives, characterization will need to be adapted to ensure that the measured rheology correlates correctly to the desired performance.

APPENDIX: Shear and Extensional Rheology Data

This appendix provides the full steady shear flow and extensional stress curves used to obtain the representational parameters used throughout this thesis.

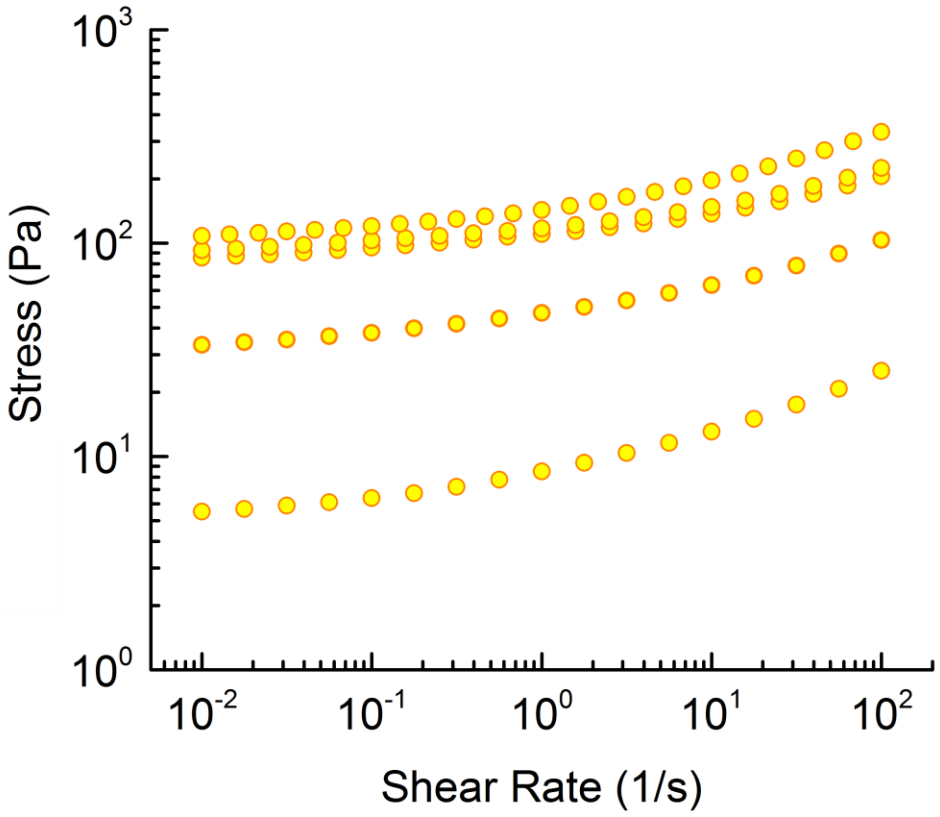

Figure A.1. Steady simple shear flow from high to low rate for Carbopol of 0.1, 0.15, 0.2, 0.25, 0.5 %wt additive. A higher concentration increases the yield stress. All tests were from high to low shear rate, and so the low-rate plateaus indicate the dynamic yield stress.

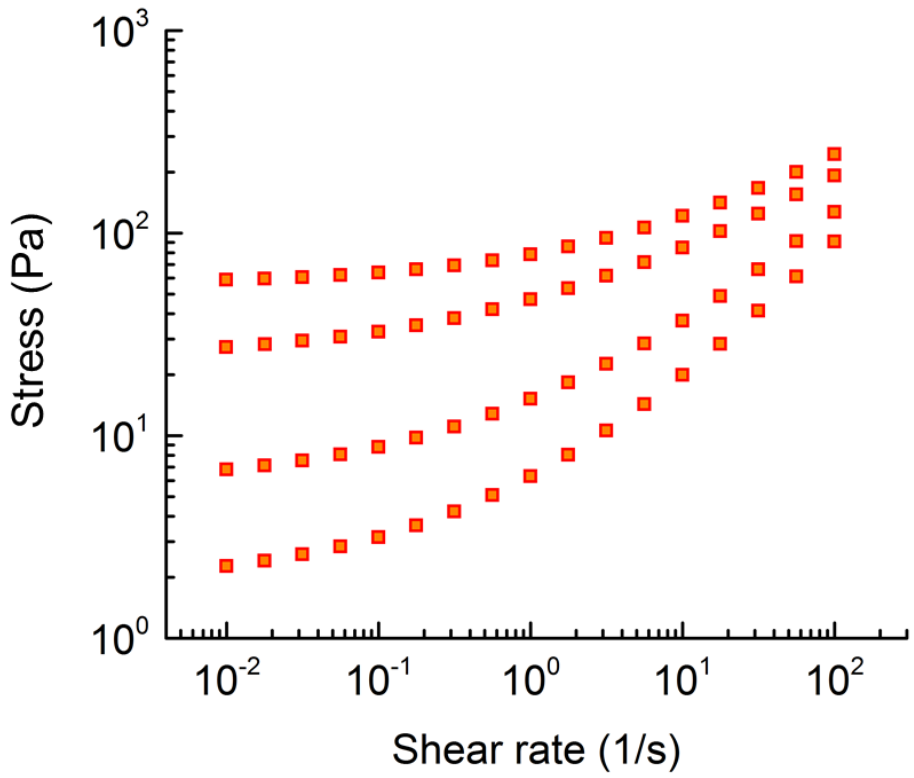

Figure A.2. Steady simple shear flow from high to low rate for silicone oil-in-water emulsion of 65, 70, 75, 80 %wt of oil. A higher concentration increases the yield stress. All tests were from high to low shear rate, and so the low-rate plateaus indicate the dynamic yield stress.

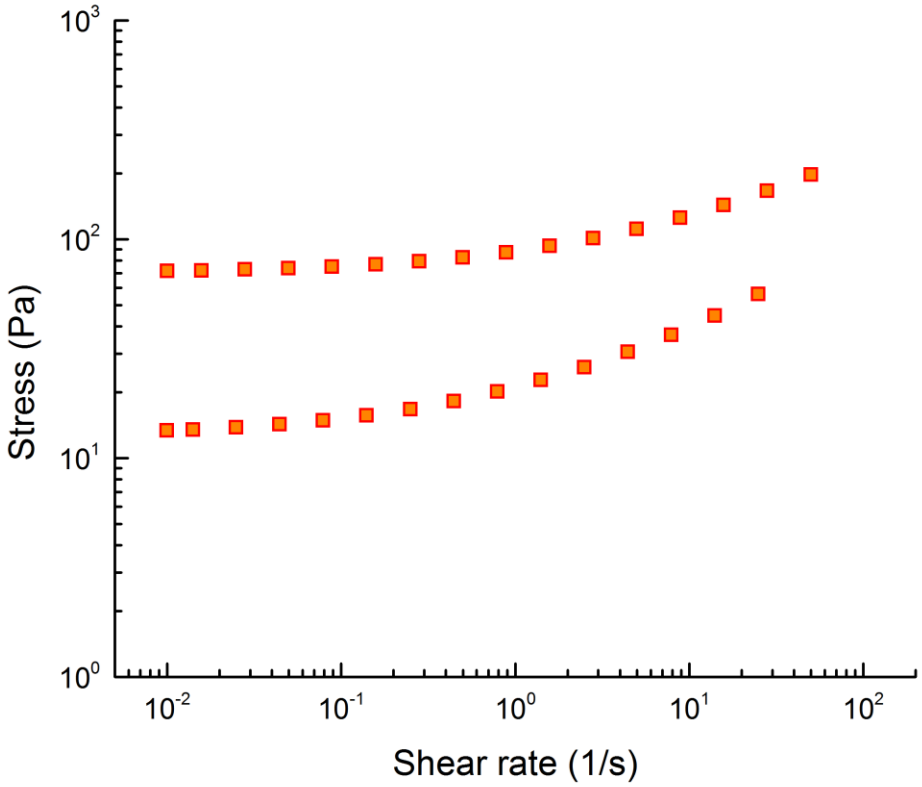

Figure A.3. Mineral oil-in-water emulsion in steady simple shear flow for 65 and 75 %wt oil. A higher concentration results in a higher yield-stress. All tests were from high to low shear rate, and so the low-rate plateaus indicate the dynamic yield stress.

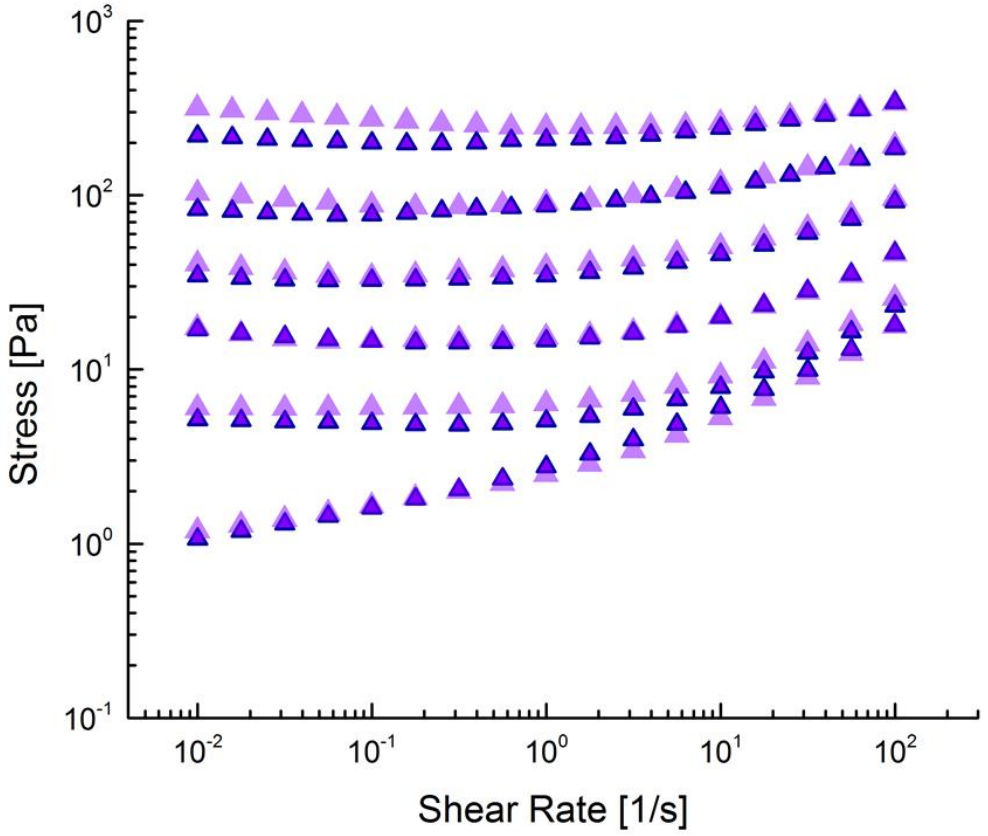

Figure A.4. Bentonite in steady simple shear flow for 7, 8, 9, 10, 11, 12 %wt. A higher concentration results in a higher yield-stress. All tests were from high to low shear rate, and so the low-rate plateaus indicate the dynamic yield stress. Highlighted curves indicate tests at a gap of 1000 µm while transparent curves were at a gap of 500 µm. Since confinement effects were observed at the smaller gap, the highlighted curves were used for all figures.

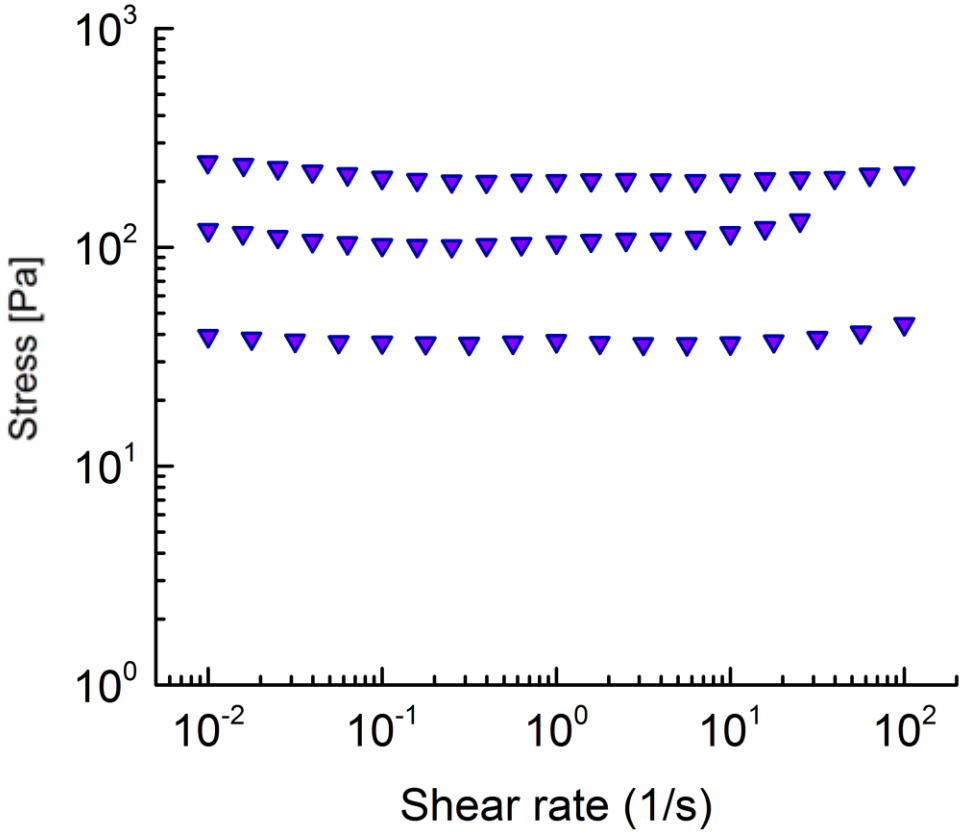

Figure A.5. Steady simple shear flow from high to low rate for Laponite of 3.5, 4, and 5%wt additive. A higher concentration increases the yield stress. All tests were from high to low shear rate, and so the low-rate plateaus indicate the dynamic yield stress.

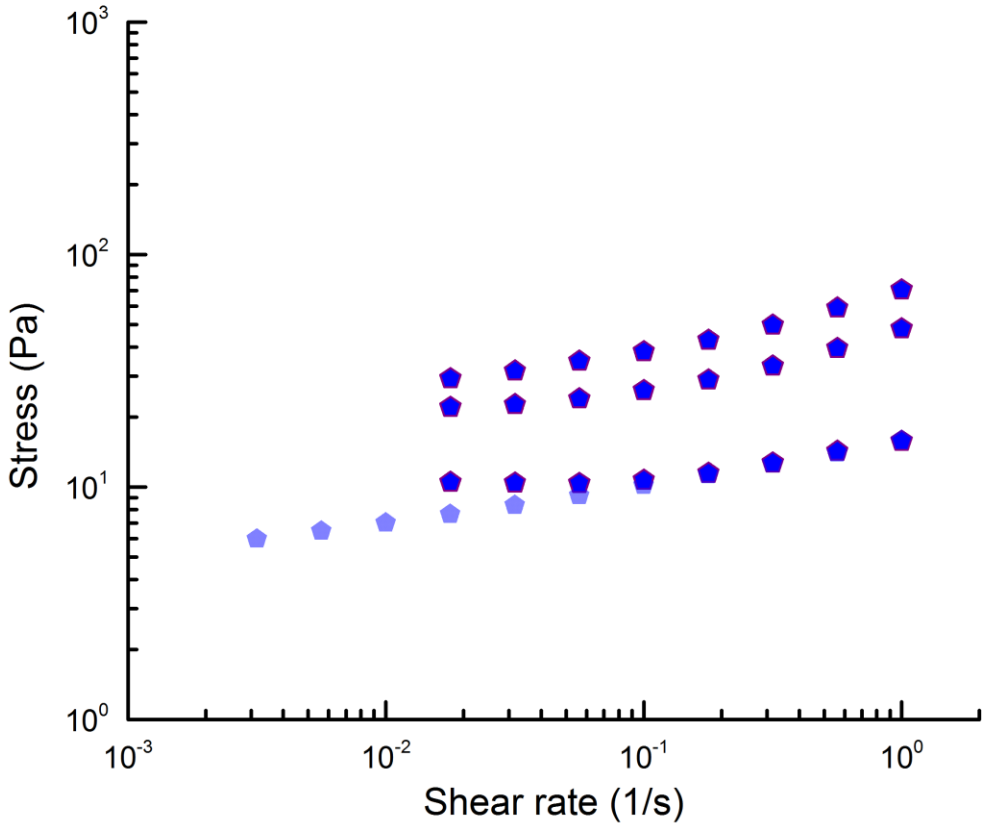

Figure A.6. Xanthan Gum in steady simple shear flow for 2, 4, 5 %wt. A higher concentration results in a higher yield-stress. All tests were from low to high shear rate, and so the low-rate plateaus indicate the *static* yield stress. High-to-low tests indicated by the transparent curve did not show a yield-stress plateau on experimental timescales.

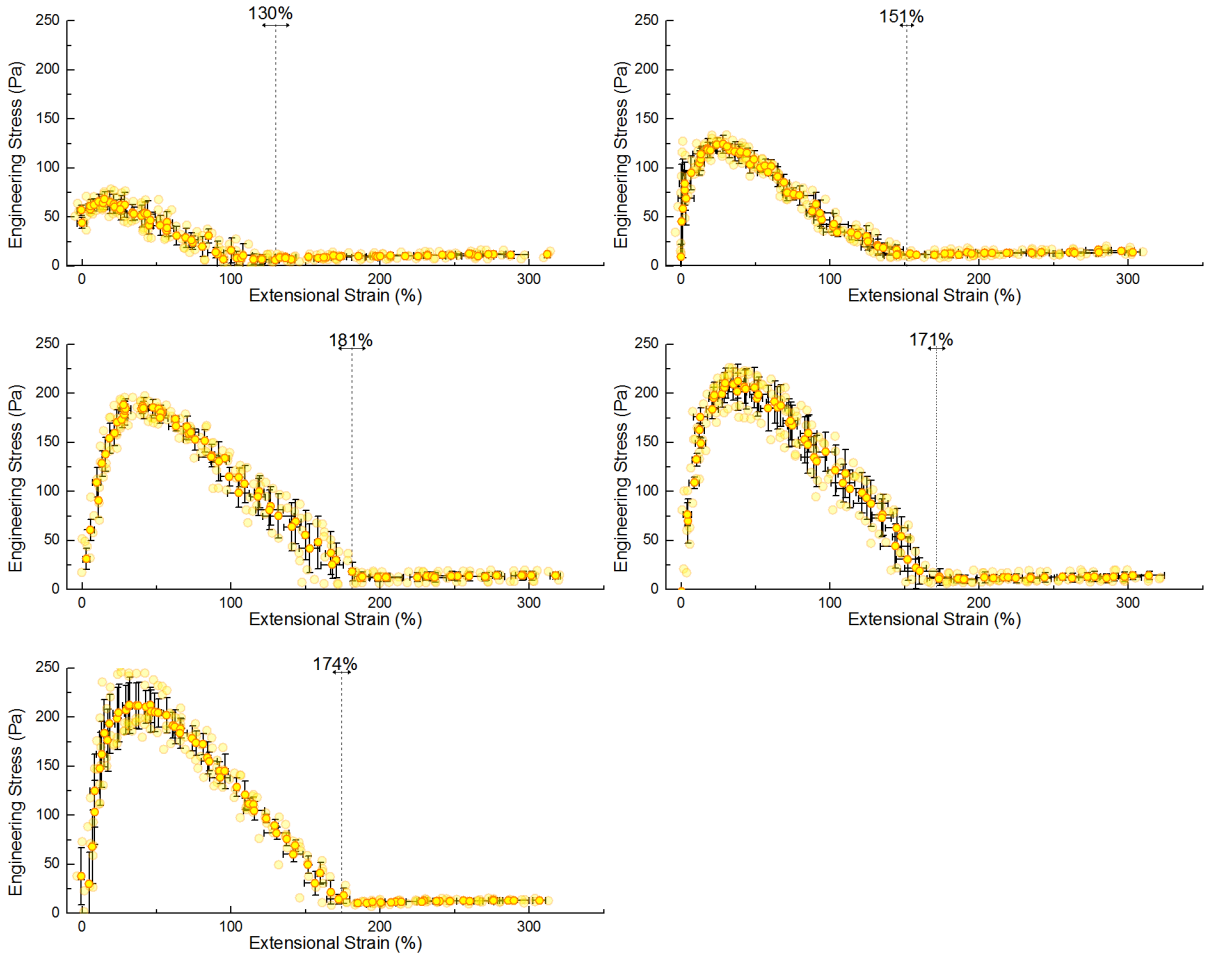

Figure A.7. Extensional engineering stress curves for Carbopol of 0.1, 0.15, 0.2, 0.25, 0.5 %wt additive from left-to-right, top-to-bottom tested using the ARES-G2 filament stretching experimental setup. The bold data points are the average of repeated experiments (faded data points) which provide the error bars. The vertical dashed lines depicts the average strain-to-break which was found by correlating the extensional stress curves with video images. The horizontal arrows below the strain-to-break labels depict the standard deviation in the strain-to-break from repeated experiments. A constant Hencky strain-rate of 0.2 was used for all extensional tests.

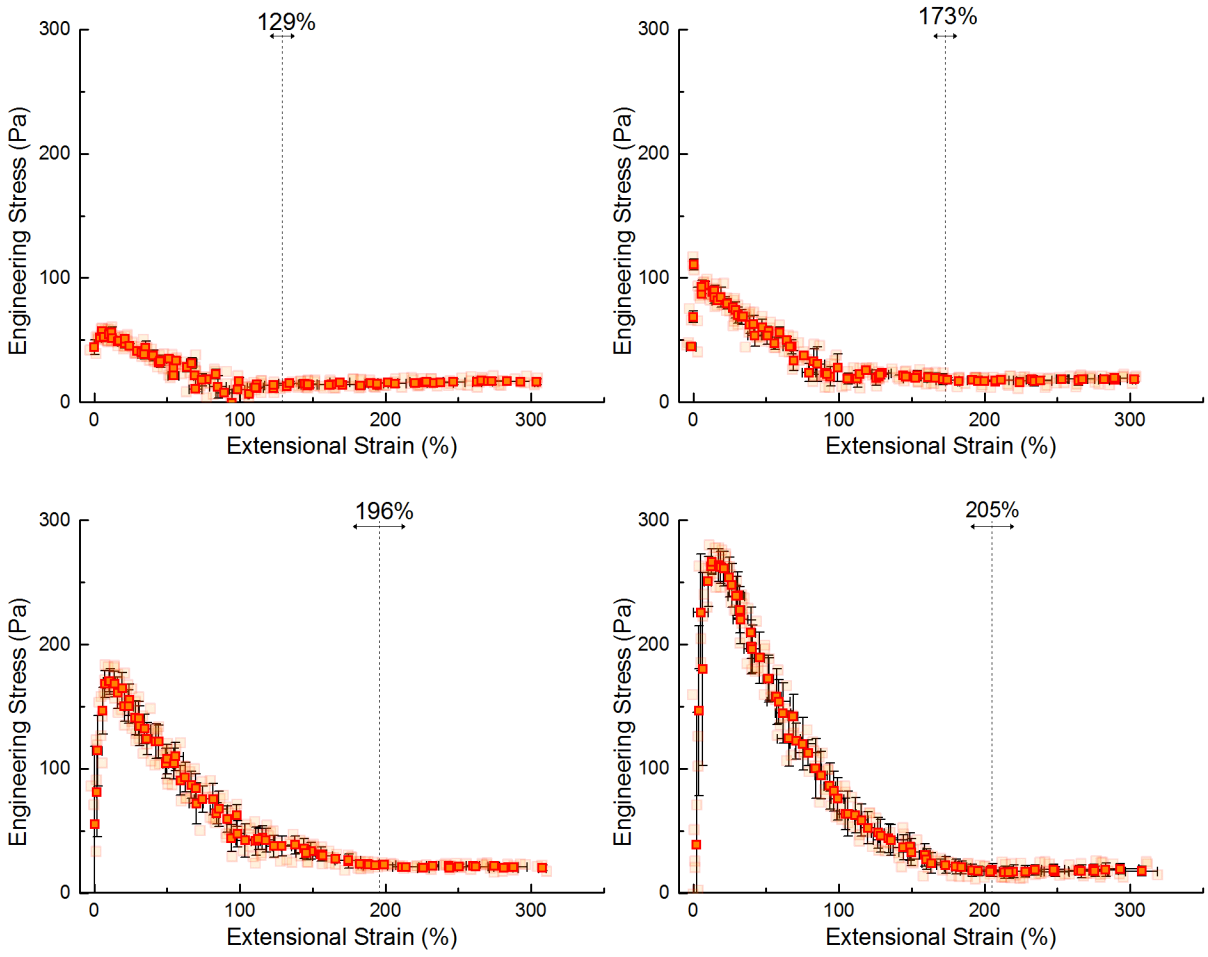

Figure A.8. Extensional engineering stress curves for silicone oil-in-water emulsions of 65, 70, 75, 80 %wt oil from left-to-right, top-to-bottom tested using the ARES-G2 filament stretching experimental setup. The bold data points are the average of repeated experiments (faded data points) which provide the error bars. The vertical dashed lines depicts the average strain-to-break which was found by correlating the extensional stress curves with video images. The horizontal arrows below the strain-to-break labels depict the standard deviation in the strain-to-break from repeated experiments. A constant Hencky strain-rate of 0.2 was used for all extensional tests.

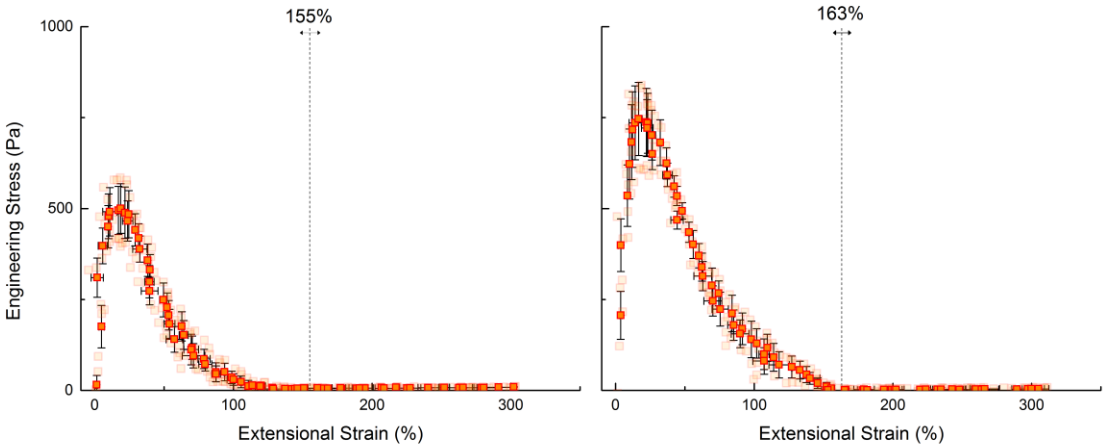

Figure A.9. Extensional engineering stress curves for mineral oil-in-water emulsions of 65, 75%wt oil from left to right tested using the ARES-G2 filament stretching experimental setup. The bold data points are the average of repeated experiments (faded data points) which provide the error bars. The vertical dashed lines depicts the average strain-to-break which was found by correlating the extensional stress curves with video images. The horizontal arrows below the strain-to-break labels depict the standard deviation in the strain-to-break from repeated experiments. A constant Hencky strain-rate of 0.2 was used for all extensional tests.

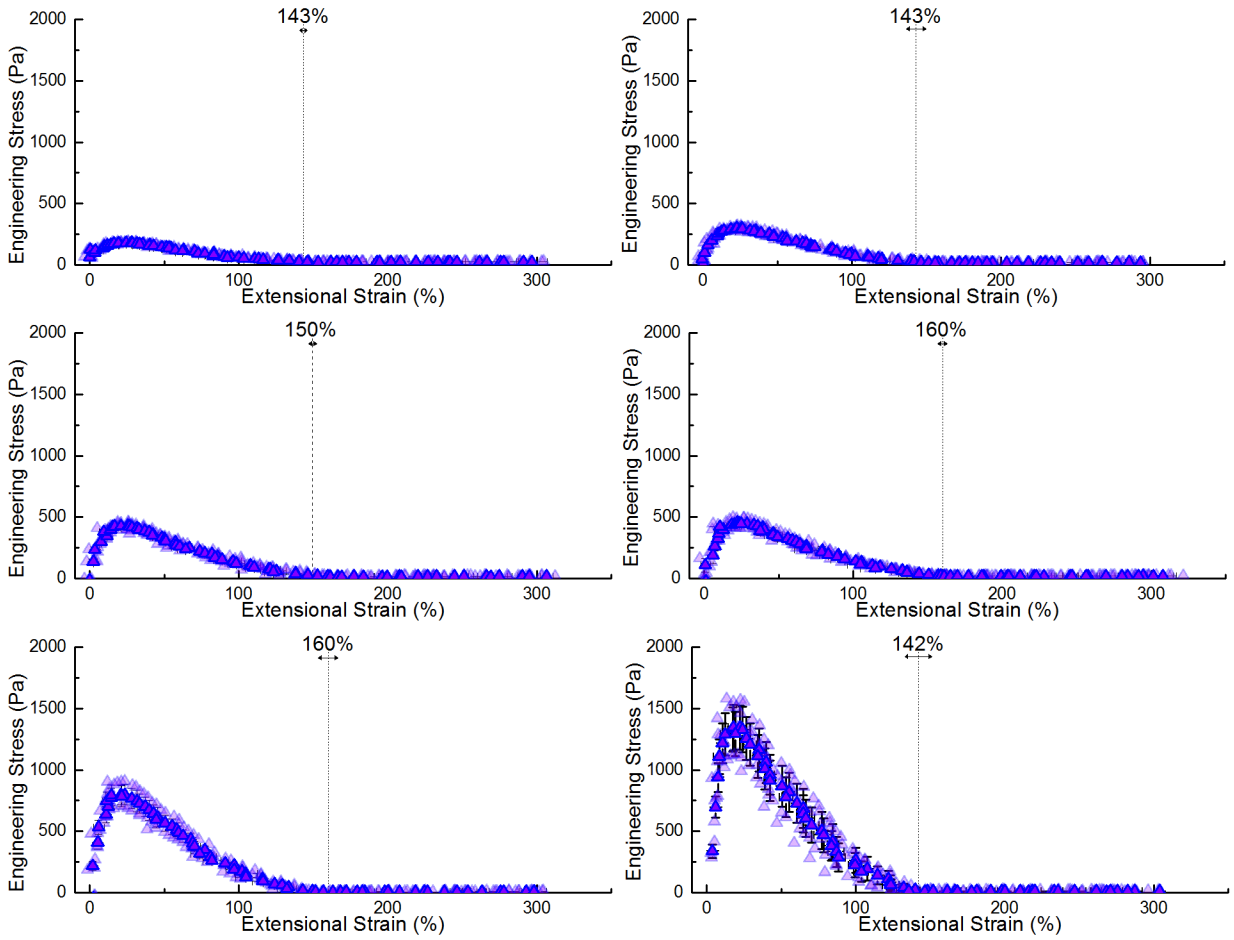

Figure A.10. Extensional engineering stress curves for Bentonite 7, 8, 9, 10, 11, 12 %wt of additive from left-to-right, top-to-bottom tested using the ARES-G2 filament stretching experimental setup. The bold data points are the average of repeated experiments (faded data points) which provide the error bars. The vertical dashed lines depicts the average strain-to-break which was found by correlating the extensional stress curves with video images. The horizontal arrows below the strain-to-break labels depict the standard deviation in the strain-to-break from repeated experiments. A constant Hencky strain-rate of 0.2 was used for all extensional tests.

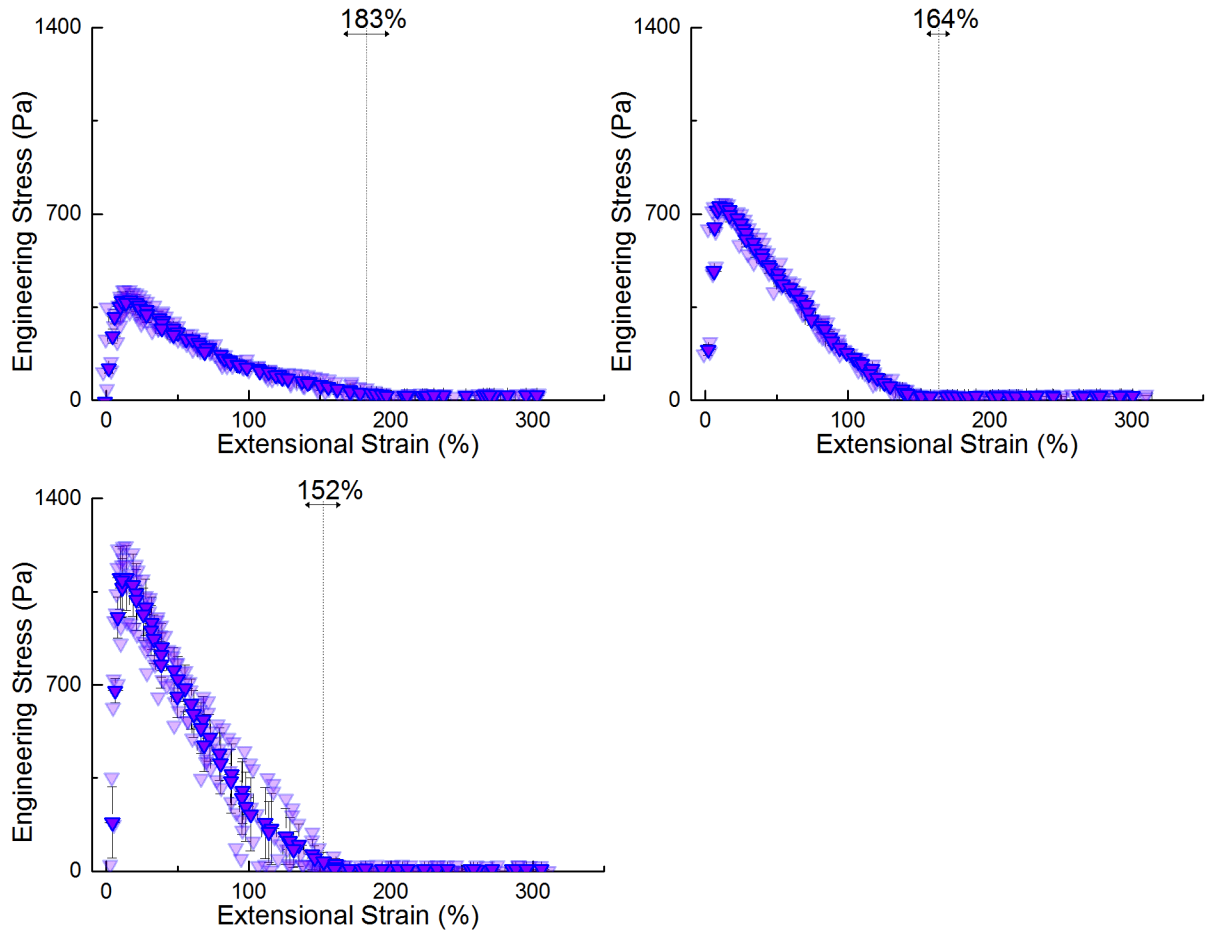

Figure A.11. Extensional engineering stress curves for Laponite 3.5, 4, 5 %wt of additive from left-to-right, top-top-bottom tested using the ARES-G2 filament stretching experimental setup. The bold data points are the average of repeated experiments (faded data points) which provide the error bars. The vertical dashed lines depicts the average strain-to-break which was found by correlating the extensional stress curves with video images. The horizontal arrows below the strain-to-break labels depict the standard deviation in the strain-to-break from repeated experiments. A constant Hencky strain-rate of 0.2 was used for all extensional tests.

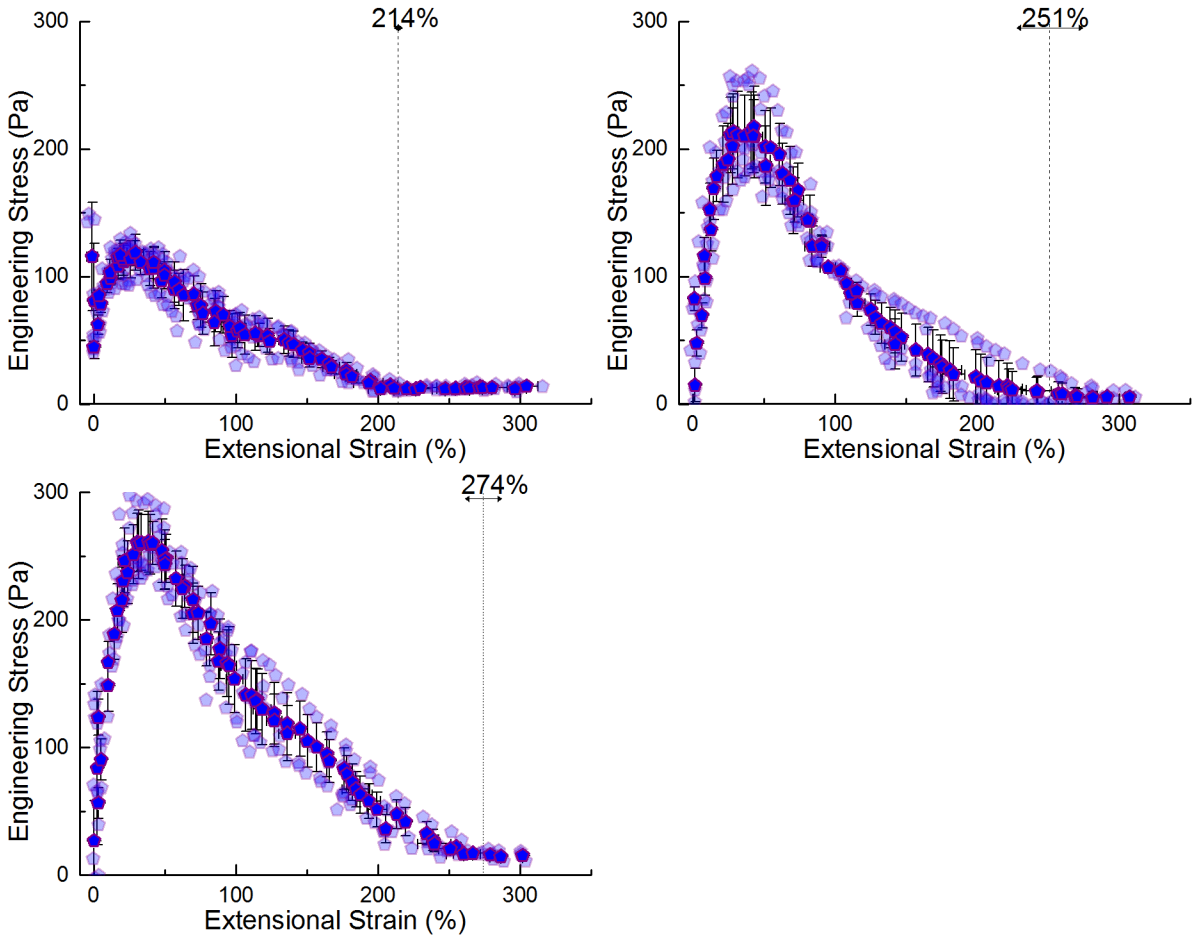

Figure A.12. Extensional engineering stress curves for Xanthan Gum of 2, 4, 5 %wt of additive from left-to-right, top-to-bottom tested using the ARES-G2 filament stretching experimental setup. The bold data points are the average of repeated experiments (faded data points) which provide the error bars. The vertical dashed lines depicts the average strain-to-break which was found by correlating the extensional stress curves with video images. The horizontal arrows below the strain-to-break labels depict the standard deviation in the strain-to-break from repeated experiments. A constant Hencky strain-rate of 0.2 was used for all extensional tests.

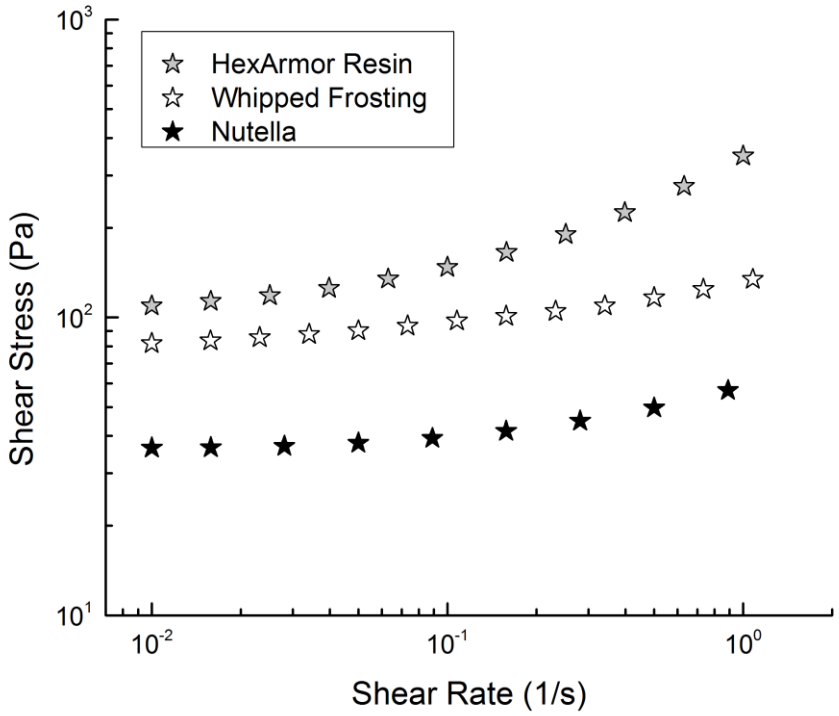

Figure A.13. Steady simple shear flow from high to low rate for three consumer products which show extensibility. All tests were from high to low shear rate, and so the low-rate plateaus indicate the dynamic yield stress.

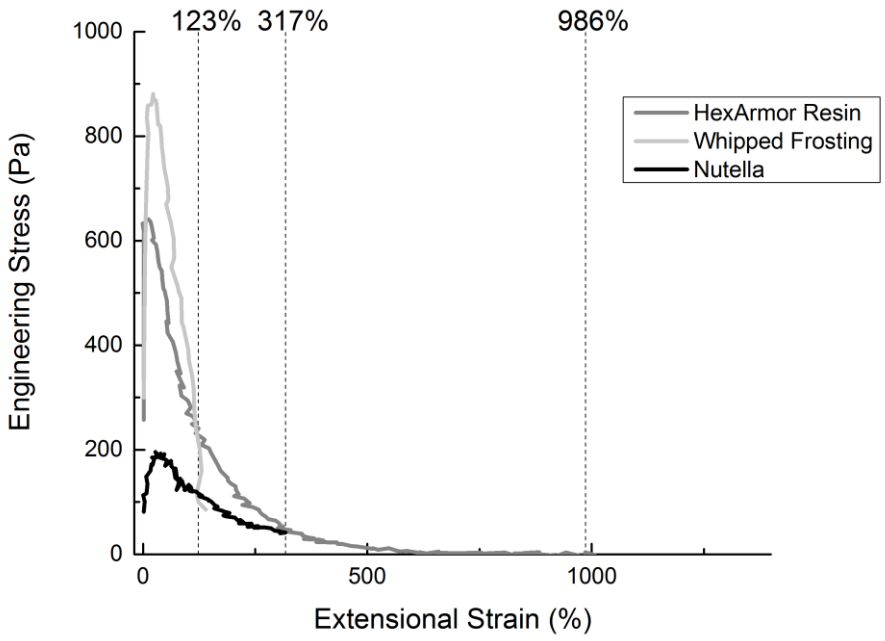

Figure A.14. Extensional engineering stress curves for three consumer products tested using the ARES-G2 filament stretching experimental setup. The vertical dashed lines depicts the average strain-to-break which was found by correlating the extensional stress curves with video images. A constant Hencky strain-rate of 0.2 was used for all extensional tests.

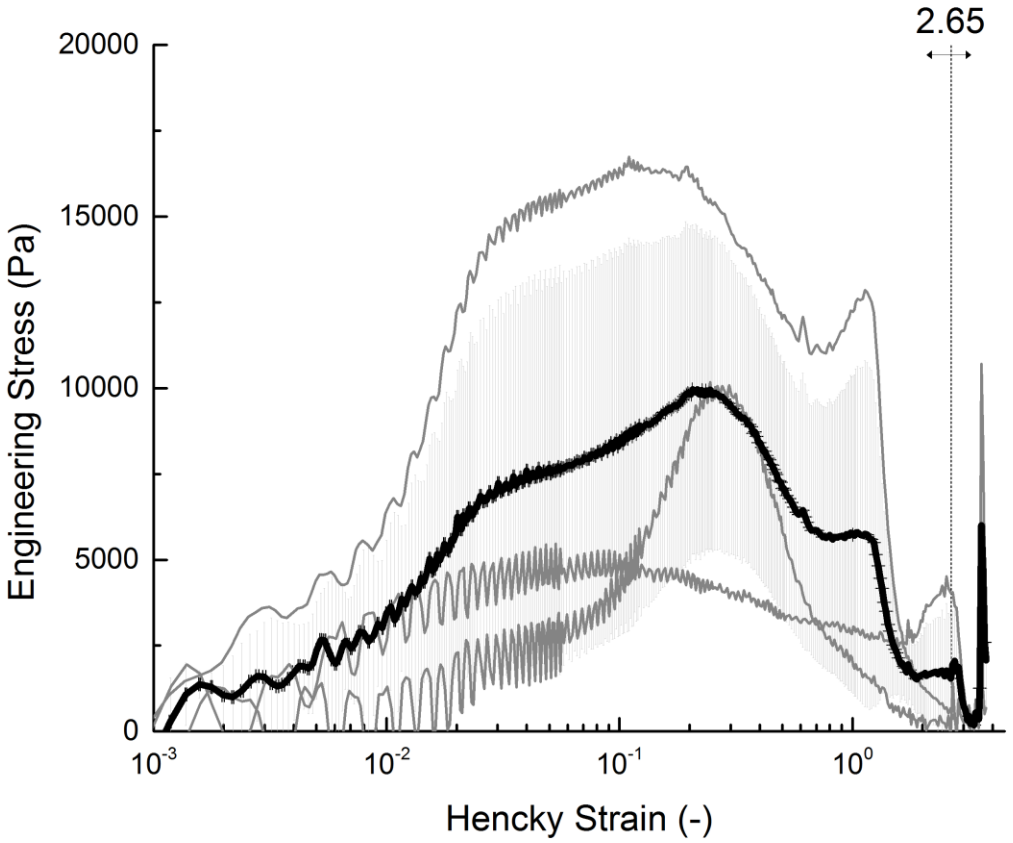

Figure A.15. Extensional engineering stress curves for three repeat experiments on Laffy Taffy at 37 °C using the SER2 counter-rotating-drum stretching experiment. The black curve shows the average of the three gray curves. For comparison with other materials, the Hencky strain was related to engineering strain with Equation (2). The vertical dashed line depicts the average strain-to-break which was found by correlating the extensional stress curves with video images. A constant Hencky strain-rate of 0.2 was used for all extensional tests.

References

[1] D. Bonn, J. Paredes, M.M. Denn, T. Divoux, C. De Recherche, P. Pascal, Yield Stress Materials in Soft Condensed Matter, arXiv. (2015) arXiv:1502.05281v1.

[2] H.A. Barnes, The yield stress — a review or " panta rhei "— everything flows ?, J. Non-Newtonian Fluid Mech. 81 (1999) 133–178. doi:10.1016/S0377-0257(98)00094-9.

[3] A. Sun, S. Gunasekaran, Yield Stress in Foods: Measurements and Applications, Int. J. Food Prop. 12 (2009) 70–101. doi:10.1080/10942910802308502.

[4] B.G. Compton, J.A. Lewis, 3D-printing of lightweight cellular composites, Adv. Mater. (2014) 5930–5935. doi:10.1002/adma.201401804.

[5] R.H. Ewoldt, C. Clasen, a. E. Hosoi, G.H. McKinley, Rheological fingerprinting of gastropod pedal mucus and synthetic complex fluids for biomimicking adhesive locomotion, Soft Matter. 3 (2007) 634. doi:10.1039/b615546d.

[6] N.J. Balmforth, I. a. Frigaard, G. Ovarlez, Yielding to Stress: Recent Developments in Viscoplastic Fluid Mechanics, Annu. Rev. Fluid Mech. 46 (2014) 121–146. doi:10.1146/annurev-fluid-010313-141424.

[7] G.B. Olson, Designing a New Material World, Science (80-.). 288 (2000) 993–998. doi:10.1126/science.288.5468.993.

[8] R.H. Ewoldt, Extremely Soft: Design with Rheologically Complex Fluids, Soft Robot. 1 (2013) 12–20. http://online.liebertpub.com/doi/abs/10.1089/soro.2013.1508 (accessed September 25, 2013).

[9] C.J. Espinoza Santos, A.Z. Nelson, R.H. Ewoldt, W.M. Kriven, Design and Fabrication of Ceramic Beads by the Vibration Method, Submitted. (n.d.).

[10] T. Bhattacharjee, S. Zehnder, K. Rowe, S. Jain, R. Nixon, G. Sawyer, et al., Writing in the Granular Gel Medium, Sci. Adv. (n.d.).

[11] E. a. Appel, M.W. Tibbitt, M.J. Webber, B. a. Mattix, O. Veiseh, R. Langer, Self-assembled hydrogels utilizing polymer–nanoparticle interactions, Nat. Commun. 6 (2015) 6295. doi:10.1038/ncomms7295.

[12] G.D. Moggridge, E.L. Cussler, Chemical Product Design, 2nd Editio, Cambridge University Press, Cambridge, 2012.

[13] K. Ulrich, S.D. Eppinger, Product design and development, 5th ed., McGraw-Hill, New York, 2012. http://www.worldcat.org/title/product-design-and-development/oclc/791505360?referer=br&ht=edition (accessed September 26, 2012).

[14] J.S. Linsey, I. Tseng, K. Fu, J. Cagan, K.L. Wood, C. Schunn, A Study of Design Fixation, Its Mitigation and Perception in Engineering Design Faculty, J. Mech. Des. 132 (2010) 041003. doi:10.1115/1.4001110.

[15] G. Pahl, W. Beitz, Engineering Design - A Systematic Approach, Springer London, London, 1996. doi:10.1007/978-1-4471-3581-4.

[16] E. de Bono, Lateral Thinking, Penguin Books, New York, NY, 1977.

[17] M. Graham, A. Slocum, R.M. Sanchez, Teaching High School Students and College Freshmen Product Development by Deterministic Design With PREP, J. Mech. Des. 129 (2007) 677. doi:10.1115/1.2722334.

[18] M.F. Ashby, Material selection in mechanical design., Fourth Edi, Butterworth-Heinemann, Boston, MA, 2011.

[19] D.D. Braun, M.R. Rosen, The Rheology Modifiers Handbook Practical Use & Application, William Andrew Publication, Norwich, N.Y., 2000.

[20] M. Ash, I. Ash, Handbook of Rheology Modifiers, Synapse Information Resources Inc., 2006.

[21] D.L. McDowell, J.H. Panchal, H.-J. Choi, C.C. Seepersad, J.K. Allen, F. Mistree, Decision Making in Engineering Design, in: Integr. Des. Multiscale, Multifunct. Mater. Prod., Elsevier, 2010: pp. 65–85. doi:10.1016/B978-1-85617-662-0.00004-1.

[22] C.C. Seepersad, R.S. Kumar, J.K. Allen, F. Mistree, D.L. McDowell, Multifunctional design of prismatic cellular materials, in: J. Comput. Mater. Des., 2005: pp. 163–181. doi:10.1007/s10820-005-3167-0.

[23] N. a. Lynd, F.T. Oyerokun, D.L. O'Donoghue, D.L. Handlin, G.H. Fredrickson, Design of soft and strong thermoplastic elastomers based on nonlinear block copolymer architectures using self-consistent-field theory, Macromolecules. 43 (2010) 3479–3486. doi:10.1021/ma902517v.

[24] H.M. Jaeger, Celebrating Soft Matter's 10th Anniversary: Toward jamming by design, Soft Matter. 11 (2015) 12–27. doi:10.1039/C4SM01923G.

[25] Q.D. Nguyen, D. V Boger, Measuring the Flow Properties of Yield Stress Fluids, Annu. Rev. Fluid Mech. 24 (1992) 47–88.

[26] P. Moller, A. Fall, V. Chikkadi, D. Derks, D. Bonn, An attempt to categorize yield stress fluid behaviour., Philos. Trans. A. Math. Phys. Eng. Sci. 367 (2009) 5139–5155. doi:10.1098/rsta.2009.0194.

[27] J.M. Piau, Carbopol gels: Elastoviscoplastic and slippery glasses made of individual swollen sponges Meso- and macroscopic properties, constitutive equations and scaling laws, J. Nonnewton. Fluid Mech. 144 (2007) 1–29. doi:10.1016/j.jnnfm.2007.02.011.

[28] W.E. Rochefort, S. Middleman, Rheology of Xanthan Gum: Salt, Temperature, and Strain Effects in Oscillatory and Steady Shear Experiments, J. Rheol. (N. Y. N. Y). 31 (1987) 337. doi:10.1122/1.549953.

[29] R.H. Ewoldt, M.T. Johnston, L.M. Caretta, Experimental challenges of shear rheology with case studies in biological complex fluids, in: S.E. Spagnolie (Ed.), Complex Fluids Biol. Syst., Springer, 2015: pp. 207–241. doi:10.1007/978-1-4939-2065-5_6.

[30] C.W. Macosko, Rheology Principles, Measurements, and Applications, Wiley, New York, 1994.

[31] F. Sciortino, Disordered materials: One liquid, two glasses., Nat. Mater. 1 (2002) 145–146. doi:10.1038/nmat752.

[32] F. Sciortino, P. Tartaglia, Glassy colloidal systems, Adv. Phys. 54 (2005) 471–524. doi:10.1080/00018730500414570.

[33] S. Manley, H.M. Wyss, K. Miyazaki, J.C. Conrad, V. Trappe, L.J. Kaufman, et al., Glasslike arrest in spinodal decomposition as a route to colloidal gelation, Phys. Rev. Lett. 95 (2005) 1–4. doi:10.1103/PhysRevLett.95.238302.

[34] V. Trappe, V. Prasad, L. Cipelletti, P.N. Segre, D.A. Weitz, Jamming phase diagram for attractive particles., Nature. 411 (2001) 772–5. doi:10.1038/35081021.

[35] B.C. Blackwell, M.E. Deetjen, J.E. Gaudio, R.H. Ewoldt, Sticking and splashing in yield-stress fluid drop impacts on coated surfaces, Phys. Fluids. 27 (2015) 043101. doi:10.1063/1.4916620.

[36] P.J. Rankin, A.T. Horvath, D.J. Klingenberg, Magnetorheology in viscoplastic media, Rheol. Acta. 38 (1999) 471–477. doi:10.1007/s003970050198.

[37] C. Chung, B. Degner, D.J. McClements, Rheology and microstructure of bimodal particulate dispersions: Model for foods containing fat droplets and starch granules, Food Res. Int. 48 (2012) 641–649. doi:10.1016/j.foodres.2012.06.011.

[38] M. Zrinyi, Intelligent polymer gels controlled by magnetic fields, Colloid Polym. Sci. 278 (2000) 98–103. doi:10.1007/s003960050017.

[39] H. McGee, On Food and Cooking: The Science and Lore of The Kitchen, Scribner, New York, NY, 2004.

[40] M. Helgeson, S. Moran, H. An, P. Doyle, Mesoporous organohydrogels from thermogelling photocrosslinkable nanoemulsions, Nat. Mater. 11 (2012) 344–352. doi:10.1038/nmta3248.

[41] S. Rose, A. Prevoteau, P. Elzière, D. Hourdet, A. Marcellan, L. Leibler, Nanoparticle solutions as adhesives for gels and biological tissues., Nature. 505 (2014) 382–5. doi:10.1038/nature12806.

[42] C. Clasen, B.P. Gearing, G.H. McKinley, The flexure-based microgap rheometer (FMR), J. Rheol. (N. Y. N. Y). 50 (2006) 883. doi:10.1122/1.2357190.

[43] R. Pal, Rheology of polymer-thickened emulsions, J. Rheol. (N. Y. N. Y). 36 (1992) 1245. doi:10.1122/1.550310.

[44] Y. Otsubo, R.K. Prud'homme, Rheology of oil-in-water emulsions, Rheol. Acta. 33 (1994) 29–37. doi:10.1007/BF00453461.

[45] T.G. Mason, J. Bibette, D.A. Weitz, Yielding and Flow of Monodisperse Emulsions, J. Colloid Interface Sci. 179 (1996) 439–448. doi:10.1006/jcis.1996.0235.

[46] Y. Takahashi, Experimental tests of the scaling relation for textured materials in mixtures of two immiscible fluids, J. Rheol. (N. Y. N. Y). 38 (1994) 699. doi:10.1122/1.550481.

[47] R.G. Larson, The Structure and Rheology of Complex Fluids, Oxford University Press, New York, NY, 1999.

[48] D.A. Weitz, J.S. Huang, SELF–SIMILAR STRUCTURES AND THE KINETICS OF AGGREGATION OF GOLD COLLOIDS, in: Kinet. Aggreg. Gelation, Elsevier, 1984: pp. 19–28. doi:10.1016/B978-0-444-86912-8.50010-9.

[49] A. Burmistrova, R. von Klitzing, Control of number density and swelling/shrinking behavior of P(NIPAM–AAc) particles at solid surfaces, J. Mater. Chem. 20 (2010) 3502. doi:10.1039/b923969c.

[50] M. Le Merrer, R. Lespiat, R. Höhler, S. Cohen-Addad, Linear and non-linear wall friction of wet foams, Soft Matter. 11 (2015) 368–381. doi:10.1039/C4SM01557F.

[51] Y.D. Liu, H.J. Choi, Electrorheological fluids: smart soft matter and characteristics, Soft Matter. 8 (2012) 11961. doi:10.1039/c2sm26179k.

[52] R. Pal, Effect of droplet size on the rheology of emulsions, AIChE J. 42 (1996) 3181–3190. doi:10.1002/aic.690421119.

[53] W. Mickel, S. Münster, L.M. Jawerth, D. a Vader, D. a Weitz, A.P. Sheppard, et al., Robust pore size analysis of filamentous networks from three-dimensional confocal microscopy., Biophys. J. 95 (2008) 6072–6080. doi:10.1529/biophysj.108.135939.

[54] M. Fuchs, M.E. Cates, Schematic models for dynamic yielding of sheared colloidal glasses., Faraday Discuss. 123 (2003) 267–286; discussion 303–322, 419–421. doi:10.1039/b205629a.

[55] R. Buscall, Effect of long-range repulsive forces on the viscosity of concentrated latices: Comparison of experimental data with an effective hard-sphere model, J. Chem. Soc., Faraday Trans. 87 (1991) 1365–1370. http://pubs.rsc.org/en/content/articlehtml/1991/ft/ft9918701365 (accessed November 6, 2013).

[56] J.R. Seth, M. Cloitre, R.T. Bonnecaze, Elastic properties of soft particle pastes, J. Rheol. (N. Y. N. Y). 50 (2006) 353. doi:10.1122/1.2186982.

[57] H. Princen, A. Kiss, Rheology of foams and highly concentrated emulsions: IV. An experimental study of the shear viscosity and yield stress of concentrated emulsions, J. Colloid Interface Sci. 128 (1989). http://www.sciencedirect.com/science/article/pii/0021979789903962 (accessed January 9, 2014).

[58] W.B. Russel, D.A. Saville, W.R. Schowalter, Rheology, in: Colloid. Dispersions, Cambridge University Press, Cambridge, 1989: pp. 456–506. doi:10.1017/CBO9780511608810.017.

[59] D.J. Klingenberg, C.F. Zukoski, Studies on the steady-shear behavior of electrorheological suspensions, Langmuir. 6 (1990) 15–24. doi:10.1021/la00091a003.

[60] J. Ginder, L. Davis, L. Elie, Rheology of magnetorheological fluids: models and measurements, Int. J. Mod. Phys. B. 10 (1996). http://www.worldscientific.com/doi/pdf/10.1142/S0217979296001744 (accessed November 6, 2013).

[61] N.J. Balmforth, N. Dubash, A.C. Slim, Extensional dynamics of viscoplastic filaments: II. Drips and bridges, J. Nonnewton. Fluid Mech. 165 (2010) 1147–1160. doi:10.1016/j.jnnfm.2010.06.004.

[62] L. Martinie, H. Buggisch, N. Willenbacher, Apparent elongational yield stress of soft matter, J. Rheol. (N. Y. N. Y). 57 (2013) 627. doi:10.1122/1.4789785.

[63] P.P. Bhat, S. Appathurai, M.T. Harris, M. Pasquali, G.H. McKinley, O. a. Basaran, Formation of beads-on-a-string structures during break-up of viscoelastic filaments, Nat. Phys. 6 (2010) 625–631. doi:10.1038/nphys1682.

[64] F.J. Galindo-Rosales, J.P. Segovia-Gutiérrez, F.T. Pinho, M. a. Alves, J. de Vicente, Extensional rheometry of magnetic dispersions, J. Rheol. (N. Y. N. Y). 59 (2015) 193–209. doi:10.1122/1.4902356.

[65] G.H. McKinley, T. Sridhar, Filament-Stretching Rheometry of Complex Fluids, Annu. Rev. Fluid Mech. 34 (2002) 375–415. doi:DOI 10.1146/annurev.fluid.34.083001.125207.

[66] M. Sentmanat, High rate extensional flow behavior of confectionery products - objectifying “mouthfeel,” in: Soc. Rheol. Annu. Meet., 2007. http://www.rheology.org/SoR07a/ViewPaper.aspx?ID=154.

[67] L. Martinetti, A.M. Mannion, W.E. Voje, R. Xie, R.H. Ewoldt, L.D. Morgret, et al., A critical gel fluid with high extensibility: The rheology of chewing gum, J. Rheol. (N. Y. N. Y). 58 (2014) 821–838. doi:10.1122/1.4874322.

[68] G.H. McKinley, A. Tripathi, How to extract the Newtonian viscosity from capillary breakup measurements in a filament rheometer, J. Rheol. (N. Y. N. Y). 44 (2000) 653. doi:10.1122/1.551105.

[69] M. Yao, G.H. McKinley, Numerical simulation of extensional deformations of viscoelastic liquid bridges in filament stretching devices, J. Nonnewton. Fluid Mech. 74 (1998) 47–88. doi:10.1016/S0377-0257(97)00052-9.

[70] D. Rees, Basic Engineering Plasticity: An Introducting With Engineering and Manufacturing Applications, Butterworth-Heinemann, 2012.

[71] R.C. Hibbeler, Mechanics of Materials, Pearson Prentice hall, 2014.

[72] M.L. Sentmanat, Miniature universal testing platform: From extensional melt rheology to solid-state deformation behavior, Rheol. Acta. 43 (2004) 657–669. doi:10.1007/s00397-004-0405-4.

[73] A. Sanz, I. Martinez, Minimum volume for a liquid bridge between equal disks, J. Colloid Interface Sci. 93 (1983) 235–240. doi:10.1016/0021-9797(83)90401-0.